

Phenocryst-poor rhyolites of bimodal, tholeiitic provinces: The Rattlesnake Tuff and implications for mush extraction models

Martin J. Streck¹ and Anita L. Grunder²

1: (corresponding author) Department of Geology, Portland State University, Portland, Or 97207-0751, USA

email: streckm@pdx.edu phone: ++1-503-725 3379 Fax: ++1-503-725-3025

2: Department of Geosciences, Oregon State University, Corvallis, OR, 97331 USA

Abstract

We consider the origin of rhyolites associated with tholeiitic basalt in bimodal provinces, as exemplified by the Rattlesnake Tuff of the High Lava Plains of eastern Oregon, in comparison to rhyolites associated with calcalkaline suites in light of recent models of extraction of rhyolite from crystal mush (Hildreth, 2004; Bachman and Bergantz, 2004). The High Lava Plains encompass a strongly bimodal, tholeiite-rhyolite suite, spatially and compositionally related to the Snake River Plain and Yellowstone Plateau. In our assessment we draw the distinction between fractionation dominated processes to make rhyolites from rhyolites and processes required to make the parental rhyolite melt.

New isotopic data and compositional zoning profiles in phenocrysts confirm that crystal fractionation dominated the generation of progressively more evolved, discrete rhyolites in the zoned Rattlesnake Tuff and are consistent with an origin of the least evolved high-silica rhyolites by partial melting of a mafic crust. While the most evolved rhyolites are compositionally virtually indistinguishable from those of calcalkaline suites, the parental rhyolites from bimodal suites are more Fe-rich than their calcalkaline counterparts. Oxygen isotope thermometry yields pre-eruptive temperatures of 860°C, in keeping with 800-880°C zircon saturation temperatures. High magmatic temperatures are common among rhyolites of bimodal suites, distinguishing them from cooler rhyolites of calcalkaline suites.

Extraction of interstitial melt from a granodioritic mush cannot produce compositions of the Rattlesnake Tuff on the basis of major and trace element arguments (especially Fe, Ba, Sr, and Eu) and on the basis of temperature considerations. Chemically viable parental crystal mushes are syenite and alkali (A-type) granites for the production of all more evolved Rattlesnake Tuff rhyolites; ferro-dacitic mush is required for production of the least-evolved, parental Rattlesnake Tuff rhyolite. Paucity of such ferro-dacitic compositions in tholeiitic

bimodal suites, especially compared to the abundance of dacitic (granodioritic) compositions in calcalkaline suites, argues against the mush extraction model for the parental rhyolite.

Furthermore, rhyolites of bimodal suites lack associated voluminous eruptions of crystal-rich ignimbrite that might represent a parental mush, as exemplified by the “monotonous intermediate” Fish Canyon Tuff in calcalkaline suites.

We conclude that extensive fractionation is common among rhyolites and may obscure their ancestry. Fe-rich parental rhyolites common in bimodal thoeiitic suites, as represented by Rattlesnake Tuff, may often be the result of partial melting of mafic to intermediate crust, in contrast to calcalkaline high-silica rhyolites that are related to voluminous suites of intermediate intrusive rocks where the pre-plutonic mush-extraction model works better.

Keywords: rhyolites, crystal-poor, melt extraction, Rattlesnake Tuff, bimodal

1. Introduction

Rhyolites have erupted in most tectonic settings ranging from oceanic to continental intraplate and volcanic arc settings to continental rift zones. Only in purely oceanic rift settings are they essentially absent. In 1933, Daly pointed out that rhyolites occur in geological settings where intermediate volcanic rocks are the most voluminous and in bimodal provinces, where basalt and rhyolite predominate. Crystal poor, highly silicic rhyolites are a ubiquitous constituent of volcanic suites that include low-silica rhyolite, and in bimodal suites they may dominate the latter. They have silica concentrations greater than 75 weight percent, at the maximum of values observed in fresh volcanic rocks (cf. Hildreth, 1981), and they typically have other geochemical indicators that suggest a history of extensive crystal fractionation. Although similar in major-element composition, high-silica rhyolites from variable tectonic settings can vary widely in

minor element and trace element, as well as isotopic characteristics. Petrotectonic classification schemes developed for granitoids have been widely applied to rhyolites (e.g., Pearce, 1984, Whalen et al., 1987, Eby, 1990). We here address the origin of crystal-poor, high-silica rhyolites that are part of a bimodal, tholeiitic basalt – rhyolite, suite of the High Lava Plains, Oregon. We contrast the origin of these rhyolites, that have affinities to A-type granites, to rhyolites associated with abundant, intermediate calcalkaline (or magnesian, Frost et al. 2001) rocks, and that have affinities with I-type granites. We will refer to the former as “bimodal” rhyolites and to the latter as “calcalkaline” rhyolites to emphasize their typical rock association.

Rhyolites of bimodal provinces, i.e. those with A-type affinities, are mainly metaluminous to mildly peralkaline (cf. Eby, 1990; Frost et al, 2001); in this regard, some comendites are considered rhyolites but the strongly peralkaline pantellerites are not (Irvine and Barragar, 1971). Rhyolites of bimodal provinces are commonly high in FeO^* and Fe^*/Mg compared to “calcalkaline” counterparts (cf. Eby, 1990; Frost et al, 2001). Mineral assemblages commonly include Fe-enriched ferromagnesian silicates and a single feldspar (anorthoclase or Na-sanidine) although two-feldspars varieties occur as well (e.g. Honjo et al., 1992). In contrast, calcalkaline rhyolites carry augite and orthopyroxene, or water-bearing ferromagnesian silicates (biotite, hornblende) and typically have two feldspars (sanidine and plagioclase).

The mechanism of generation of high-silica rhyolite is not easily extracted from the minerals they carry. Many high-silica rhyolites are sparsely phyrlic to aphyric. The minerals largely represent equilibrium assemblages, and so are suited to tracking the pre-eruptive magmatic state of the liquid rather than giving clues to the origin of the high-silica melt. We here distinguish between the problems of generating geochemical variability among syn-eruptive high-silica rhyolites, i.e. rhyolites that can be found as distinct compositions in single

pyroclastic deposits, (e.g., Hildreth, 1979, Streck and Grunder, 1995) and the origin of the least-evolved high-silica rhyolite in a cogenetic suite.

The distinctive, highly silicic composition invites search for a common process leading to all such high-silica rhyolites. Here, we focus on petrological distinctions between high silica rhyolites associated with intermediate magmatism and high-silica rhyolites related to bimodal suites. We undertake the comparison in the context of the Rattlesnake Tuff from eastern Oregon, which is an example of a voluminous, crystal-poor, high-silica rhyolite system that is part of a bimodal, basalt-rhyolite province. We present new data and review existing data bearing on the petrogenesis of the Rattlesnake Tuff and use these to consider a mush extraction model, that is gaining popularity to explain crystal-poor, high-silica rhyolites in general (Bachmann and Bergantz, 2004, Hildreth, 2004). We find that melt extraction from a granodioritic mush cannot produce either the parental Rattlesnake rhyolite, nor the compositional variation among rhyolite. Extraction from a syenitic to alkali granite mush is a viable chemical model for differentiation among rhyolites. The estimated ferro-dacitic composition of the mush that would have to exist to produce the parental Rattlesnake rhyolite is uncommon in the High Lava Plains and in the geologic record, suggesting alternative models of generation of parental, least-evolved rhyolite in bimodal suites.

2. Tectonic and Geochemical Context

2.1 High Lava Plains

The Rattlesnake Tuff was erupted 7.1 My ago from a vent area in the western Harney Basin, a part of the High Lava Plains of Oregon (Fig. 1) (Streck and Grunder 1995). Late-Miocene to Quaternary volcanism of the High Lava Plains is strongly bimodal with rhyolite

erupted as dome complexes and ignimbrites and basalt and basaltic andesite erupted as widespread lavas typically a few m to 10 m thick (Fig. 1; Jordan et al., 2002). Based on estimates of areal extents and thickness, mafic rocks and rhyolites are subequal in volume on the High Lava Plains. Intermediate compositions are scarce (Fig. 1b) and, where they occur, they are mainly simple mixtures of mafic and rhyolitic magmas (Linneman and Myers, 1990, Streck and Grunder, 1999, Johnson and Grunder, 2000).

The High Lava Plains define the western portion of a broad Late Cenozoic basaltic province that extends from the Cascades eastward to Yellowstone and that includes the Owyhee Plateau and the Snake River Plain. Silicic volcanism of the High Lava Plains defines a northwestward-younging magmatic trend (MacLeod et al., 1976; Jordan et al., 2004) that makes a mirror image to the northeastward age progression of silicic volcanism of the Snake River Plain and Yellowstone Plateau (Christiansen and Yeats 1992; Pierce and Morgan, 1992, Humphreys et al. 2000).

Eruption of high-alumina olivine tholeiites (HAOT) flows was preceded in the eastern High Lava Plains by mid-Miocene intermediate lavas (Walker 1979; MacLean 1994; Jordan et al., 2004) and mid-Miocene Steens Basalt. The Steens Basalt is part of the ~17-15 Ma flood basalt event that includes the Columbia River Basalt and dikes of the Northern Nevada Rift (Fuller 1931; Gunn and Watkins 1970; Johnson et al., 1989; Hooper et al., 2002; Camp and Ross, 2004).

Rhyolites from the High Lava Plains are metaluminous to mildly peralkaline. Most are high-silica rhyolites (> 75 wt. % SiO₂) with low MgO (< 0.2 wt. %) and CaO (< 0.8 wt. %) concentrations combined with molar (Na+K)/Al of greater than 0.9. Mafic magmatism across the High Lava Plains is dominated by high-alumina olivine tholeiite (HAOT) and fractionated

basaltic andesitic lava flows (Hart et al. 1984; Streck and Grunder, 2002; Jordan et al., 2002).

The basalts typically have 48-49 wt. % SiO₂, 18-16 wt. % Al₂O₃, 10-8 wt. % MgO and 0.1-0.3 wt.% K₂O (examples in Table 1).

2.2 The Rattlesnake Tuff

The Rattlesnake Tuff eruption produced a single thin (10-30+ m) cooling unit of which depositional remnants are found as far as 150 km north- and southward from the postulated vent (Streck and Grunder, 1995). This ranks the Rattlesnake Tuff among the farthest traveled pyroclastic flows currently known (Wilson et al., 1995). The tuff is mainly (99 %) made of variably colored and welded high-silica rhyolite ash and pumice that define five distinct compositional clusters (rhyolites A through E). Mingling of rhyolites and minor dacite and mafic magma during this extremely violent eruption led to a spectacular mixture of differently colored glass shards in the matrix and to an assemblage of variously colored homogeneous pumices and banded (layered) pumices. Darker bands (black, gray, brown or red) include rhyolites C, D and E and dacite; white bands are rhyolites A and B (Streck and Grunder, 1997; 1999).

Although eruptive mixing is pervasive, some depositional features indicate a tapping sequence from early most-evolved rhyolite (rhyolite composition A) to later less evolved rhyolite, dacite, and finally basalt. Rare precursor pyroclastic fall deposits contain only white pumices that are compositionally akin to most-evolved rhyolite A (Streck and Grunder, 1997). The basal meter and distal portions of the tuff commonly also contain only white pumices and white shards. Overlying tuff is darker indicating more admixture of dark rhyolites. Sparse, but ubiquitous dark dacite pumices are found in proximal to mid-distal localities (< ~80 km).

Basaltic inclusions are restricted to proximal locations, indicating that onset of tapping of basaltic magmas was during waning stages of the eruption.

Mafic magma occurs as streaks of phenocryst-poor basaltic andesite mingled with rhyolite-dacite banded pumices and as round blobs of phenocryst-rich basalt in mostly dacitic pumices (Streck and Grunder, 1999). Textures suggest that basalt was quenched owing to greater temperature contrast with the silicic host while basaltic andesite mingled with dacite and rhyolite magmas. The widespread syn-eruptive mixing of rhyolite A through E, dacite, and basaltic andesite liquids during ascent and deposition indicates that the melts were in close spatial association. The width of diffusion profiles between layers of white and dark rhyolitic magma suggests that banded pumices were quenched within 100s of seconds of mingling (Pendergast et al., 2000).

2.3 Rattlesnake Tuff: Magma Compositions

Glass shards and pumice clasts of the Rattlesnake Tuff have significant compositional gradients between least evolved high-silica rhyolite (rhyolite E) with 75.3 wt. % SiO_2 (average; Streck and Grunder, 1997) and most evolved high-silica rhyolite (rhyolite A) with 77.4 wt. % SiO_2 (average; see representative samples in Table 1).

Rhyolite compositions E through A are established by clustering of analyses from single unbanded pumices and from glass shards of the matrix into groups suggesting that gradients were stepwise within the pre-eruptive, zoned high-silica rhyolite portion of the Rattlesnake magma chamber. The modest bulk compositional range accompanies a two-fold enrichment in the most incompatible elements Rb and Cs and a 77-fold depletion in Ba based on compositional averages of rhyolite A and E (Streck and Grunder, 1997). Rhyolites D, C, and B have successively

enriched or depleted compositions intermediate between rhyolites E and A (Fig. 2) (Streck and Grunder, 1997). Exceptions are elements that have minimal variations across the high-silica rhyolite compositional spectrum or for which potential gradients are masked by analytical error. The degree of enrichments or depletions towards more evolved compositions varies for different elements, which leads to curved trends, or rarely looped trends, on element-element diagrams (Fig. 2).

Dacite pumice clasts are variably banded with minor high-silica rhyolite and basaltic andesite (Streck and Grunder, 1999). Also, the compositions of dacite pumices with less than 10% banding (i.e. those reflecting largely true dacite magma) lie on mixing trends between the least-evolved of the high-silica rhyolites (E or D) and incompatible element-enriched, basaltic andesitic compositions as recorded by phenocyst-poor inclusions. Neither most-evolved high-silica rhyolite nor regional olivine tholeiites are directly involved in the mixing to yield dacite magma (Fig. 2; Streck and Grunder, 1999). The composition of dacites indicates that least evolved high-silica rhyolites and basaltic andesites, were juxtaposed in the pre-eruptive reservoir.

2.4 Rattlesnake Tuff: Mineralogical Data

All rhyolitic compositions are extremely phenocryst poor ranging from ~1 volume % crystals in rhyolite E to aphyric in rhyolite A. The main minerals are alkali feldspar, quartz and clinopyroxene and lesser fayalitic olivine. Accessory phases are titanomagnetite, zircon, apatite, and chevkinite (Streck and Grunder, 1997). In more evolved compositions, alkali feldspar are poorer in Na, Ba and Eu, clinopyroxenes are less Fe rich, but richer in Mn and Sc, and titanomagnetites are poorer in Ti and Ta (Fig. 3, Table 2). These trends are based on bulk

compositional data representing ~50 to 300 hand picked crystal composites, as well as electron microprobe spot analyses (Streck and Grunder, 1997).

Phenocrysts in basaltic inclusions are dominantly olivine and plagioclase with subordinate clinopyroxene. Fresh olivine ranges from Fo₈₀ to Fo₇₂ and Ni from 1200 to 700 ppm, plagioclase ranges from An₈₁ to An₅₁ and augite has a narrow range with Wo₄₂En₄₅Fs₁₃ to Wo₃₇En₄₂Fs₂₁ and Cr contents range from 3400 ppm to 600 ppm. Dacite pumices are also phenocryst poor (ca. 2%) and contain mostly phenocrysts derived from rhyolites and basaltic magmas, based on compositional similarities. Some clinopyroxenes in dacite are intermediate in composition between those from rhyolitic and basaltic magma and appear to have crystallized from hybrid dacite (Streck and Grunder, 1999).

3. Results

3.1 Isotope data

Sr-, Nd-, and Pb-isotope data were obtained for four samples of Rattlesnake Tuff, viz., pumices of rhyolites E and A, dacite pumice and a basaltic inclusion, as well as for four basaltic and two rhyolitic lavas erupted in the western Harney Basin area (Fig. 4, Table 1). Burns Butte rhyolite lava predates and Juniper Ridge rhyolite lavas postdate the tuff. Of the four samples of mafic volcanic rocks in the area, two represent ambient high-alumina olivine tholeiite, one of which erupted immediately post-Rattlesnake Tuff and the other is younger than western Juniper Ridge (5.7 Ma), based on stratigraphic relationships. Two basaltic andesites, one of calcalkaline and one of tholeiitic affinity (differentiated on the basis of their respective Fe/Mg ratios), were also included. Together these samples are a fair representation of the range of compositions of the western Harney Basin.

With respect to Pb isotope ratios, the two Rattlesnake Tuff samples are the same, cluster closely with other rhyolites and are slightly elevated in radiogenic Pb relative to more mafic constituents in the area (Fig. 4). With respect to covariation of $^{143}\text{Nd}/^{144}\text{Nd}$ and $^{87}\text{Sr}/^{86}\text{Sr}$, the Rattlesnake Tuff samples (dacite, mafic inclusion, and rhyolite E) are the same, but rhyolite A is more strongly displaced toward elevated $^{87}\text{Sr}/^{86}\text{Sr}$ at virtually the same $^{143}\text{Nd}/^{144}\text{Nd}$. Values for ϵNd of 3.5 and 3.4 for brown and white Rattlesnake Tuff shards, respectively, were determined by Nash (B. Nash, pers. comm.), in keeping with values reported here.

Taken together, the western Harney Basin suite Sr-Nd isotope variation defines a general crustal contamination trend with HAOT lavas pinning the end with high $^{143}\text{Nd}/^{144}\text{Nd}$ and low $^{87}\text{Sr}/^{86}\text{Sr}$. Isotope ratios for the two HAOT samples are virtually the same and match that of tholeiitic basaltic andesite. In contrast, calcalkaline basaltic andesite is displaced toward crustal compositions. Rhyolites, however, are variable in $^{87}\text{Sr}/^{86}\text{Sr}$ composition. Those with lowest Sr concentration (Rattlesnake Tuff rhyolite A, 2 ppm, and Burns Butte, 14 ppm) are also the most elevated in $^{87}\text{Sr}/^{86}\text{Sr}$ (Table 1), reflecting the sensitivity of such compositions to contamination. Excepting these samples, the western Harney Basin suite has little isotopic variation.

Oxygen isotope analyses were done in duplicate by laser fluorination, at Washington State University, for quartz and titanomagnetite separates from high-silica rhyolite C (sample 165A; see Streck and Grunder, 1997 for bulk chemical composition). Quartz yielded $\delta^{18}\text{O}_{\text{SMOW}}$ values of 7.80 and 7.57 ‰ (± 0.2 ‰), and titanomagnetite yielded $\delta^{18}\text{O}_{\text{SMOW}}$ of 2.78 and 2.71 ‰. Isotopic fractionation between quartz and titanomagnetite ($\Delta_{\text{Qz-Mt}} = 4.9$) indicates a magmatic temperature of 850°C to 860°C (using Chiba et al., 1989 and Clayton and Kieffer, 1991, respectively) consistent with zircon saturation temperature estimates of 860°C (Streck and

Grunder, 1997). The oxygen isotopic composition of the melt was 7.2, based on $\Delta_{\text{quartz-silicic glass}}$ values of 0.4 at 900°C to 0.6 at 700°C (Matthews et al., 1994).

3.2 Mineral zoning data

Detailed mineral zoning profiles were obtained from electron microprobe traverses from center to rim across selected clinopyroxene and alkali feldspar crystals (Fig. 5). Individual crystals are essentially unzoned in major constituents, and have small, oscillatory variation in minor constituents. New microprobe data confirm the compositional trends in mineral composition that attend bulk rock trends described above, but indicate compositional overlap between rhyolite groups. In particular, rhyolite D contains minerals with compositions overlapping with those found in rhyolite E and C (Figs. 5, 6) indicating similar growth conditions or inheritance. Nevertheless, distinct equilibrium phenocryst populations exist, as suggested by crystals of uniform composition combined with euhedral shape, and define a stepwise compositional gradient among distinct and related rhyolite liquids.

4. Discussion

In the following discussion, we first treat rhyolites of the Rattlesnake Tuff and compare them to rhyolites of the Harney Basin and High Lava Plains in general. We then consider the origin of Rattlesnake Tuff rhyolite in light of recent models of extraction of high-silica rhyolite from vast reservoirs of crystal mush. The main inference is that crystal fractionation processes among Harney Basin rhyolites lead ultimately to daughter rhyolitic compositions that are virtually indistinguishable from rhyolites of calcalkaline suites. It is therefore essential to compare among least-evolved, parental rhyolites to understand magmatic histories of rhyolites.

4.1 Rhyolites of the Rattlesnake Tuff

In order to produce the range of rhyolites from E to A, Streck and Grunder (1997) proposed a model of ~50% fractionation of a phenocrystic mineral assemblage with a greater proportion of quartz and feldspar relative to mafic minerals than proportions observed in the mode. A small amount of crustal assimilation was modeled based on increases in highly incompatible element ratios from E to A, such as Rb/Ta, Cs/Ta, and U/Ta, assuming equal incompatibility during fractionation (Streck and Grunder, 1997). The radiogenic isotope data bear out the fractionation dominated model, in that Pb- and Nd-isotope ratios are essentially unchanged from E to A, and Sr-isotope ratios in low-Sr (2 ppm) rhyolite A are consistent with a minor crustal influence. The new crystal zoning data are also consistent with the existence of discrete and related high-silica rhyolite liquids closely juxtaposed in the magma reservoir. Rhyolite D, while clearly distinct in bulk composition and Or content of alkali feldspar (Figs. 3, 6), appears to have affinities with rhyolites C and E, as indicated by compositionally overlapping populations of alkali feldspar and clinopyroxene phenocrysts among C, D and E (Figs. 5, 6). Also, rhyolites C, D, and E have more compositional overlap on elemental variation diagrams compared to the distinct clusters defined by rhyolites A and B. In summary, rhyolite E is the least evolved rhyolite and spawned sequential distinct intermediate rhyolites D, C and B, and ultimately the most evolved rhyolite A. It is therefore primarily rhyolite E that must be considered in order to understand the origin of Rattlesnake Tuff rhyolite in the context of generation of crystal-poor rhyolites of this bimodal suite.

$\delta^{18}\text{O}$ of rhyolite C melt of 7.2 ‰ is modestly elevated compared to basalts in general, which are clustered around 6‰ (Taylor, 1968; Taylor and Sheppard, 1986), and compared to Pleistocene basalts in the region (5.2 to 6.9‰, average 5.8‰, Medicine Lake, Donnelly-Nolan,

1998). $\delta^{18}\text{O}$ of rhyolite may reflect a protracted fractionation history from basalt, which causes about 1‰ increase (Taylor and Sheppard, 1986) or derivation by partial melting of mafic crust. The overall displacement of all Rattlesnake Tuff ejecta to higher Sr- and Pb-isotope ratios and lower Nd-isotope ratios relative to regional, primitive basalts argues for an origin by crustal melting (cf. Streck, 2002). On the other hand, the crust must be quite young and mafic, in light of the limited isotopic variability.

4.2 Rhyolites of the Harney Basin and High Lava Plains

High-silica rhyolites of the High Lava Plains are aphyric to sparsely phytic, bearing Nannidine or anorthoclase, while lower silica varieties commonly contain up to ~10% phenocrysts and have plagioclase (Linneman and Myers, 1990, MacLean, 1994, Streck and Grunder, 1997; Johnson and Grunder, 2000). The rhyolites of the Rattlesnake Tuff span about half of the range of compositions of rhyolites of the High Lava Plains with respect to major and minor elements (Fig. 7, and Fig. 6 in Streck, 2002), but equal or exceed the range with respect to trace elements.

We attribute the scatter in compositions among High Lava Plains rhyolites to at least three different causes. First, as exemplified by the trend in the Rattlesnake Tuff, crystal fractionation causes sharp declines in Ba and Eu/Eu^* (feldspars) and FeO^* (mafic phases) as compositions collapse to a small range at highest SiO_2 . Thus High Lava Plain rhyolites indicate variable degrees of differentiation from other rhyolites (Fig. 7). Second, the path by which rhyolites reach greater degree of differentiation varies, because even the most evolved rhyolites (i.e. $\text{SiO}_2 > 76$ wt.%, Ba of < 100 , and $\text{Eu}/\text{Eu}^* < 0.3$) have a wide range, indeed the entire observed range of FeO^* (from 0.8 to 3.2 wt.%). Third, the high-silica rhyolites are derived from a variety of parental rhyolites. Least fractionated rhyolites, those with the highest Eu/Eu^* (0.6),

range in SiO₂ from 70 to 75 wt.%. These cannot be related to one another by fractionation involving feldspar, and so imply the existence of different parent rhyolites.

The parental rhyolites, in turn, probably reflect variable small degrees (5-20 %) of melting of mafic crustal rocks, by analogy to the history of the Rattlesnake Tuff rhyolite (Streck, 2002). Melting of mafic crustal rocks is consistent with the isotopically primitive character of rhyolites. Values of $^{87}\text{Sr}/^{86}\text{Sr}_i$ are 0.7040 ± 0.0003 for 9 high-silica rhyolites spanning the entire High Lava Plains (Walker, 1981, Jordan, 2001, and this study) with 3 additional (low-Sr) samples ranging to as high as 0.7060 (Burns Butte, this study and Johnson, 1995). Primitive High Lava Plains basalts range from ~ 0.7035 to 0.7040 and Middle Miocene basalts in the region have values spanning 0.7034 to 0.7045, with the higher values in the easternmost portion (Hart and Carlson, 1987; Brandon and Goles, 1995, Jordan, 2001, and Table 1). The composition of mafic protoliths that produced rhyolitic liquids experimentally by 5-20 % melting are comparable to basaltic compositions of the High Lava Plains (Beard and Lofgren, 1991; Sisson et al., 2005). Sisson et al. (2005) found that at low (QFM) oxygen fugacities, silicic melts with (70 to 75 wt. % SiO₂) can have up to 2.5 to 3 wt.% FeO*. FeO* concentrations are lower and K₂O concentrations higher in silicic liquids produced at more oxidizing conditions.

When Rattlesnake Tuff and other High Lava Plains rhyolites are compared to rhyolites from calcalkaline associations (Figs. 7, 8), the most fractionated rhyolites overlap in composition, but most High Lava Plains rhyolites are distinguished by higher FeO* at a given SiO₂, Ba, or Eu/Eu*. This re-emphasizes the point that for the discussion of generation models for rhyolites it is of great importance to keep in mind the degree of evolution of the erupted rhyolite because prior protracted fractionation may obscure its rhyodacitic to rhyolitic ancestry.

4.3 Crystal mush as a nursery for high-silica rhyolites

Rhyolite generation models can be generally grouped by the two principal mechanisms: partial melting of the crust and fractional crystallization from less evolved magmas. Models for generation of chemical gradients within voluminous rhyolites erupted as ignimbrites have ranged from differentiation within single magma chambers (e.g., Hildreth, 1979; Mahood, 1981; Michael, 1983; Cameron, 1984; Streck and Grunder, 1997) to juxtaposition of separate rhyolite magma batches shortly prior to eruption (e.g., Mills et al., 1997). Workers who proposed models operating in single reservoirs have invoked a wide variety of differentiation processes, although mineral-liquid equilibria have regained overwhelming acceptance in recent years as the dominating process to induce elemental enrichment or depletion patterns. The question has been returned to where and how mineral-liquid fractionation processes take place. For example, crystals and liquids may be fractionated in boundary layers of convecting chambers, by microsettling, or by filter pressing (e.g., Sparks et al., 1984; Miller et al., 1988) in order to introduce chemical gradients within magmatic reservoirs. A model of melt extraction from crystal mush (Hildreth, 2004, Bachmann and Bergantz, 2004) has recently gained attention, in which liquid evolution takes places throughout a crystallizing magma body followed by expulsion of the differentiated liquid(s) to produce crystal-poor rhyolite (ibid.). The general idea is that as batches of granodioritic magma reach crystallinities of 40-50% during cooling the remaining interstitial melt becomes high-silica rhyolite. Escape of this interstitial melt from different regions of the mush and accumulation on top of the grandodioritic magma produces a crystal-poor melt cap which may follow its own differentiation history. This model requires extremely voluminous ($>2000 \text{ km}^3$) magma batches of crystal mush in order to produce hundreds of km^3 of crystal poor high-silica rhyolite, such as the Bishop Tuff. Enormous crystal-rich

monotonous intermediate (dacitic) ignimbrites, such as the ~5000 km³ Fish Canyon Tuff, are thought to be the erupted equivalent of such mushes (Bachmann et al, 2002) and reflect the existence of granitoid batholith ancestry to high-silica rhyolite melts of calcalkaline association. The relatively close match of composition of matrix glass of the Fish Canyon Tuff to Bishop Tuff-like compositions makes the mush extraction model compelling (Fig. 8). But can it work to make the more Fe-rich liquids that distinguish high-silica rhyolites of the bimodal, tholeiitic association? Our intent below is to provide details about the applicability of this model using the Rattlesnake Tuff as a case study.

4.4 Problems with melt extraction model from granodioritic mush for rhyolites of bimodal, tholeiitic suites

The appeal for linking crystal-rich tuffs of the monotounous intermediate type with the eruption of phenocryst-poor, high-silica rhyolite magma through a melt-extraction model is that the glass compositions of monotounous tuffs share many attributes with erupted high-silica rhyolite magma. These attributes include CaO and MgO of <0.7 wt.%, low Al₂O₃ (<14 wt.%), and of course SiO₂ >75 wt.%. Although such melt is remarkably similar in major elements to high-silica rhyolites of the Rattlesnake Tuff an important difference is that the least-evolved rhyolite of the Rattlesnake Tuff, i.e. rhyolite E, is more than twice as Fe-rich as any interstitial melt of monotounous intermediate tuffs we could find (Fig. 8). Rhyolite E contains 1.96±0.09 wt. % FeO* versus a range of ~0.4-0.66 wt. % FeO* for data from the Fish Canyon Tuff, Lund Tuff, and Atana Tuff (Lindsay et al., 2001; Bachmann et al., 2002; Maughan et al. 2002; E. Christiansen, pers. Communication, “this volume”). Elevated Fe also distinguishes most High Lava Plains rhyolites (Fig.7), as well as other crystal-poor high-silica rhyolites of bimodal

associations (Fig 8). In particular, rhyolites from the Snake River Plain and Yellowstone Plateau are also of the Fe-rich type. The elevated Fe in rhyolites of bimodal tholeiitic provinces is a fundamental feature, but can become obscured by fractionation, as seen in rhyolite A of the Rattlesnake Tuff.

Another compositional difference is that the $\text{Na}_2\text{O}/\text{K}_2\text{O}$ ratio is lower (0.6-0.8) in glass of monotonous ignimbrites than in rhyolite E (~1) and other rhyolites from bimodal suites. This is suggested by the composition of glassy melt inclusions from the Fish Canyon Tuff (Johnson and Rutherford, 1989) compared to glasses of rhyolite E samples with the least low-temperature Na/K exchange. Interpretation of alkali ratios requires caution owing to their susceptibility to alteration.

Trace-elemental features of the Rattlesnake Tuff further support that rhyolite E was not extracted from a crystallizing granodioritic magma. Samples of rhyolite E indicate a narrow range of Ba/Rb, between 25 and 30. The liquid fraction in granodioritic mush may be affected by partial remelting processes when mush experiences thermal rejuvenation and crystallization during cooling. Regardless of the process that imparts greater control, the Ba/Rb of bulk mush will always be higher than (or at best equal to) the Ba/Rb of the liquid because Ba is always less (or at best equally) incompatible than Rb in intermediate to silicic magmas. Thus, bulk "mush" would have to have Ba/Rb higher or at least equal to the least-evolved Rattlesnake Tuff rhyolites. A survey of typical granodiorites or "monotonous" ignimbrites reveals that none have Ba/Rb ratio close to those observed in rhyolite E. Selected rock suites have following Ba/Rb ratios: Fish Canyon Tuff: 5-10 (bulk), ~2 (glass) (Bachmann et al., 2002, 2005); Lund Tuff: 5-9 (bulk) (Maughan et al., 2002); Atana Tuff: 2.8-4 (bulk), 0.3-1.7 (glass) (Lindsay et al., 2001);

granodiorites of Palisade Crest intrusive suite: 6-13 (Sawka et al., 1990); I-type granodiorites of Lachlan fold belt: 3-9 (Chappell and White, 1992).

Another trace-elemental argument in support of why granodiorite mush is unsuitable as a "rhyolite E" nursery, is based on how Ba behaves with regard to Sr during the generation from rhyolite E to rhyolite A. The depletion during differentiation of rhyolite E to A is 77-fold in Ba but only 12-fold in Sr (Streck and Grunder, 1997), that is, Ba decreases much faster than Sr from rhyolite E to A. Note that although XRF data of Sr at ~2 ppm levels may be viewed with caution, isotopic dilution measurements confirm XRF data of Sr (Table 1). Feldspar crystallization is the dominant control on systematics of Ba and Sr in intermediate to silicic magmas, since feldspars dominate the mineral assemblage. Both elements are very compatible to weakly compatible in alkali-feldspar and plagioclase, albeit Ba becomes incompatible in plagioclase at An of greater than about 45 (cf. Blundy and Wood, 1991). No other phases can induce large changes in Ba/Sr during rhyolite differentiation either because both elements are very incompatible (e.g. quartz) or volumetrically insignificant (e.g. biotite). A stronger decrease in Ba compared to Sr can be achieved during sole removal of sanidine, which can have a greater partition coefficient for Ba than for Sr (cf. Bachmann et al., 2005). Removal of plagioclase in addition to sanidine would make it increasingly more difficult to reduce Ba faster than Sr. Along these lines, Ba/Sr is higher in glass of crystal rich ignimbrites than in bulk tuff. Select rock suites have following Ba/Sr ratios: Fish Canyon Tuff: ~1.8 (bulk), ~4.5 (glass) (Bachmann et al., 2002, 2005); Atana Tuff: ~2 (bulk), ~4 (glass) (Lindsay et al., 2001). This indicates that plagioclase removal is significant, leading to a stronger depletion of Sr than Ba during the crystallization of granodioritic crystal mush. This is exactly opposite to the behavior of Ba and Sr in the Rattlesnake Tuff. Ba/Sr in the Rattlesnake Tuff decreases from rhyolite E to A and does not

increase, as observed in bulk-glass pairs of monotonous ignimbrites (Fig. 9). While the proportion of sanidine to plagioclase likely increases in calcalkaline, granodioritic magmas towards higher crystallinity, plagioclase crystallization does not cease during the last 40-50% crystallization. This is suggested by the mineralogy of cognate holocrystalline granodioritic fragments in comparison with Fish Canyon Tuff (cf. Bachmann et al., 2002). Also, high-silica rhyolite melt inclusion data indicate $(\text{Na}+\text{K})/\text{Al}$ is less than one and therefore plagioclase is likely to continue to crystallize even though CaO is extremely low (Scaillet and MacDonald, 2001). Thus the crystallization sequence of granodioritic crystal mushes is inconsistent with a stronger decrease in Ba than Sr (Fig.9).

Beside chemical arguments, we can make a strong argument based on temperature why typical calcalkaline crystal-rich dacitic magmas cannot be the parent to Rattlesnake Tuff rhyolites and other, similar rhyolites from bimodal provinces. The eruption temperature of the Fish Canyon Tuff is between 700-800°C (Whitney and Stormer, 1985; Bachman et al., 2002). In contrast, our previous temperature estimates suggest that rhyolite E was 880°C, which conforms with our new estimate of 860°C for rhyolite C. More extreme temperature differences from monotonous ignimbrites are found for example in the rhyolites from the Snake River Plain where eruptive temperatures are mostly in excess of 950°C (Honjo et al., 1992). In other words, high-silica rhyolites from bimodal provinces are too hot to have resided in a mush with 50% or greater crystallinity with granodioritic bulk composition. Below we consider whether Rattlesnake rhyolite E could have been extracted from a different mush.

4.5 Constraints for rhyolite extraction scenarios and alternative models

In pursuing a mush extraction model there are several possibilities. The entire fractionation process might occur during progressive crystallization from 50% crystals to 95%

crystals in a "mush-sponge continuum", accompanied by successive episodes of melt-escape to create a compositionally zoned cap, as envisioned by Hildreth (2004). Or, high-silica rhyolite might be produced first and chemical gradients within it might be due to separate processes after melt expulsion (Bachmann and Bergantz, 2004). While typical granodioritic mush fails as a suitable source to derive rhyolite E, we can consider what other composition mush at 50% crystallinity might exist to yield the least-differentiated rhyolite upon melt extraction. This magma body would have needed to undergo crystallization yielding an interstitial melt with high Ba (~1900 ppm) but low Sr (~25 ppm) and relatively high Eu/Eu* (~0.6) (Table 1, also Streck and Grunder, 1997). Furthermore, the magma would need to be at rather reducing conditions yet quite fractionated to induce high FeO*/MgO of ~20 in rhyolite E. Thus it would be a magma of tholeiitic affinity with a bulk composition of a ferro-dacite. Such compositions exist in the Rattlesnake Tuff as sparse dacitic pumices. Elsewhere the best matches are Fe-rich latites (59-65 wt.% SiO₂) and quartz-latites (65-72 wt.% SiO₂), such as in the Parana-Etendeka flood-basalt province (e.g. Bellieni et al., 1986; Kirsten et al., 2000; Ewart et al., 2004). In the case of the Harney Basin, petrographic and geochemical details indicate that the rare Fe-rich intermediates were produced mainly by mixing of basaltic and rhyolitic liquids (Streck and Grunder, 1999; Johnson and Grunder, 2000) and also through assimilation of felsic melt by basalt, coupled with fractionation (MacLean, 1994). Thus the intermediates are not the cause but rather the consequence of the existence of a rhyolite, which is emphasized by their minuscule volumes compared to rhyolites and basaltic rocks. Rare voluminous examples of Fe-rich intermediate magmas (Ewart et al., 2004) range from aphyric to 20% crystals. Voluminous examples of dacite compositions in basalt-rhyolite suites are rare while intermediate rocks dominate calcalkaline suites – in volcanic as well as plutonic suites. In short, it is conceivable that crystal mush of such

“ferro-dacitic” bulk compositions might exist and possibly have the right chemical characteristics to yield rhyolite E after melt extraction. Yet, the geological record, or better the lack thereof, argues against it.

To account for the internal variations among Rattlesnake Tuff rhyolite E to A, we previously calculated that differentiation of rhyolite E would produce syenitic cumulates in the fractionation step from rhyolite E to D and low-silica to high-silica alkali-granites for subsequent steps (cf. Table 7 in Streck and Grunder, 1997). Such compositions are indeed found abundantly in A-type plutonic provinces and so generally make suitable plutonic counterparts to large bimodal volcanic provinces such as the High Lava Plains or Yellowstone Plateau (Christiansen, 2001). Accumulation of progressively more differentiated rhyolitic liquids into a growing, crystal-poor cupola by melt extraction episodes from an underlying syenitic to alkali granite mush system can account for chemical variability in the rhyolites of the Rattlesnake Tuff, analogous to the model proposed for calcalkaline rhyolites (Hildreth, 2004). On the other hand, a (quartz-) syenitic composition would not be a suitable alternative to the above mentioned “ferro-dacite” to make rhyolite E upon melt extraction, thus making the single mush hypothesis more difficult to reconcile. It is unlikely that, if sanidine crystallizes, as would be the case in a syenitic mush, a Ba/Sr of ~70-90, as observed in rhyolite E (Streck and Grunder, 1997), could be produced or at least maintained in the evolving interstitial melt of the crystallizing mush (see above). A survey of syenite occurrences (e.g. Eby et al., 1992) indicate Ba concentrations and Ba/Sr ratios mostly lower than in rhyolite E.

5. Conclusions

Nearly aphyric rhyolites of the Rattlesnake Tuff are part of a late Miocene-Pliocene bimodal, rhyolite-basalt province of the High Lava Plains of eastern Oregon. Rhyolites from the

High Lava Plains are geochemically diverse but indicate mineralogical and compositional features that are typical for A-type rhyolites from bimodal provinces in general. High-silica rhyolites of the High Lava Plains are enriched in FeO* compared with crystal-poor, calcalkaline rhyolites, but extensive crystal fractionation can render evolved rhyolites of distinct parentage and association nearly indistinguishable. The most evolved, nearly aphyric rhyolites of the Rattlesnake Tuff are essentially identical to those of calcalkaline suites. It is thus essential to consider the degree of differentiation when considering the ancestry of high-silica rhyolites.

New mineral data on the voluminous high-silica rhyolites from the Rattlesnake Tuff strengthen our prior analysis indicating that a sequence of five discrete and progressively more differentiated rhyolite melts erupted virtually simultaneously to produce a single, widespread ignimbrite cooling unit. The temperature of 860°C obtained from oxygen-isotope fractionation between quartz-magnetite pair for intermediate rhyolite, is consistent with the previous range of zircon saturation temperatures of 800°C to 880°C for most to least evolved rhyolite, respectively. Least and most evolved rhyolite are nearly identical in Pb- and Nd-isotope composition, and most-evolved rhyolite (low-Sr) rhyolite has slightly elevated values. These data are consistent with crystal fractionation dominated differentiation among rhyolites with minor crustal contamination. A slight shift in radiogenic isotope data to more crustal values in Rattlesnake Tuff ejecta compared to regional primitive high-alumina olivine tholeiites, and $\delta^{18}\text{O}$ of 7.2 ‰ of the rhyolite, suggests origin of the least-evolved and most Fe-rich Rattlesnake Tuff rhyolite by melting of mafic crust.

The recently proposed model to explain the latter through melt extraction from granodioritic mush (Hildreth, 2004; Bachmann and Bergantz, 2004) cannot apply to the Rattlesnake Tuff inasmuch as granodiorite mush parent cannot yield least-evolved Rattlesnake

rhyolite, nor explain the differentiation trend among different Rattlesnake rhyolites. While a syenitic and alkali granitic residual mush can be reconciled with compositional trends *among* Rattlesnake rhyolites, a ferro-dacitic mush would be required to produce the least-evolved Rattlesnake Tuff rhyolite. Yet, the paucity of such ferro-dacitic compositions in tholeiitic bimodal suites, especially compared to the abundance of dacitic (granodioritic) compositions in calcalkaline suites, argues against the mush extraction model for the parental rhyolite. Also, ferro-dacitic compositions have not erupted to produce analogs to the voluminous, monotonous intermediate tuffs, such as the Fish Canyon Tuff, which in turn is an eruptive analog of the parental granodioritic mush to calcalkaline rhyolite. Finally, the high magmatic temperatures of the Rattlesnake Tuff and similar rhyolites of bimodal suites are difficult to reconcile with extraction from largely crystallized intermediate composition mush.

Compositional diversity among the High Lava Plains rhyolites is largely attributable to variable degrees of crystal fractionation among rhyolites, coupled with variability among parental rhyolites. Slight variations in the crustal composition and a range of degrees of melting (about 5-20%) of the mafic crust can account for regional variability in parental rhyolite. Partial melting of mafic crust to yield least-evolved rhyolites, followed by differentiation to produce more evolved rhyolites, is consistent with petrologic arguments as well as the geological record for rhyolites of the High Lava Plains, Oregon. Similar scenarios, but extending protolith composition to include more felsic compositions (e.g., Skjerlie and Johnston, 1992, 1993), may yield “A-type” rhyolites of other bimodal tholeiitic suites.

6. Acknowledgements

We thank Jenda Johnson, Brennan Jordan, Jim MacLean and Kaleb Scarberry for cooperative work on the High Lava Plains, in the lab, and in the office. Bruce Nelson and Peter

Larsen provided access to their isotope laboratories. We thank Henrietta Cathey and Olivier Bachmann for thoughtful reviews and Eric Christiansen for additional review comments as well as editorial handling of the manuscript. We also thank Mike McCurry, Eric Christiansen and Bill Leeman for facilitating the present rhyolite volume. This research was supported in part by NSF grants EAR-9220500 to A. Grunder and A. Deino and EAR-9725166 to A. Grunder, R. Duncan, and D. Graham. Furthermore, part of this work was supported through the Graduiertenkolleg funds at former GEOMAR, Kiel during a post-doctoral stay of Streck.

References

- Bachmann, O., Bergantz, G.W., 2004. On the origin of crystal-poor rhyolites: Extracted from batholithic crystal mushes. *J. Petrol.* 45, 1565-1582.
- Bachmann, O., Dungan, M.A., Lipman, P.W., 2002. The Fish Canyon magma body, San Juan volcanic field, Colorado; rejuvenation and eruption of an upper crustal batholith. *J. Petrol.* 43, 1469-1503.
- Bachmann, O., Dungan, M.A., Bussy, F., 2005. Insights into shallow magmatic processes in large silicic magma bodies: the trace element record in the Fish Canyon magma, Colorado. *Contrib. Mineral. Petrol.* 149, 338-349.
- Beard J.S., Lofgren G.E., 1991. Dehydration melting and water-saturated melting of basaltic and andesitic greenstones and amphibolites at 1, 3, and 6.9 kb. *J Petrol* 32: 365-401
- Bellieni, G., Comin-Chiaramonti, P., Maruques, A.J., Melfi, A.J.R., Nardy, C., Papatrechas, E.M., Piccirillo, A., Roisenberg A., Stolfa., D., 1986. Petrogenetic aspects of acid and basaltic lavas from the Parana Plateau (Brazil): geological, mineralogical and petrological relationships. *J. Petrol.* 27, 915-944.

- Blundy JD, Wood BJ, 1991. Crystal-chemical controls on the partitioning of Sr and Ba between plagioclase feldspar, silicate melts, and hydrothermal solutions. *Geochim Cosmochim Acta* 55: 193-209.
- Brandon, A.D., Goles, G.G., 1995, Assessing subcontinental lithospheric mantle sources for basalts: Neogene volcanism in the Pacific Northwest, USA as a test case. *Contrib. Min. Petrol.* 121, 364-379.
- Cameron, K., 1984. Bishop Tuff revisited; new rare earth element data consistent with crystal fractionation. *Science*, 224, 1338-1340.
- Camp, V.E., and Ross, M.E., 2004. Mantle Dynamics and genesis of mafic magmatism in the intermontane Pacific Northwest. *J. Geophys. Res.* 109, BO8204, doi:10.1029/2003JB002838/2004
- Chappell, B.W., White, A.J.R., 1992. I- and S-type granites in the Lachlan Fold Belt. *Trans. Roy. Soc. Edin. Earth Sciences*, 83, 1-26.
- Cathey, H.E., Nash, B.P., 2004. The Cougar Point Tuff: Implications for thermochemical zonation and longevity of high-temperature, large-volume silicic magmas of the Miocene Yellowstone Hotspot. *J. Petrol.* 45, 27-58.
- Chiba, H., Chacko, T., Clayton, R.N., Goldsmith, J.R., 1989. Oxygen isotope fractionation involving diopside, forsterite, magnetite, and calcite- application to geothermometry. *Geochim. Cosmochim. Acta* 53, 2985-2995.
- Christiansen, R.L., 2001. The Quaternary and Pliocene Yellowstone Plateau volcanic field of Wyoming, Idaho, and Montana. *U.S. Geol. Surv. Prof. Pap* 729-G

- Christiansen, R.L., Yeats, R.S., 1992. Post-Laramide geology of the US Cordilleran region. In: Burchfiel BC, Lipman PW, Zoback ML (eds). The Cordilleran orogen: Conterminous US, Geology of North America. Geol Soc Am, Boulder, Colorado G-3, pp 261-406
- Clayton, R.N., Kieffer, S.W., 1991, Oxygen isotopic thermometry calibration. Spec. Pub. Geochem. Soc. 3, 3-10.
- Daly, R.A., 1933. Igneous rocks and their depths of the Earth. Hafner Press, New York, pp 1-589 (reprinted 1968)
- Donnelly-Nolan, J.M., 1998. Abrupt shift in $\delta^{18}\text{O}$ values at the medicine Lake Volcano (California, USA). Bull. Volcanol. 59, 529-536.
- Eby, G.N., 1990. The A-type granitoids: A review of their occurrence and chemical characteristics and speculations on their petrogenesis. Lithos 26, 115-134.
- Eby, G.N., Krueger, H.W., Creasy, J.W., 1992. Geology, geochronology, and geochemistry of the White Mountain batholith, New Hampshire. Geol. Soc. Am. Special Paper 268, 379-397.
- Ewart, A., Marsh, J.S., Milner, S.C., Duncan, A.R., Kamber, B.S., Armstrong, R.A., 2004. Petrology and geochemistry of early Cretaceous bimodal continental flood volcanism of the NW Etendeka, Namibia. Part 2: Characteristics and petrogenesis of high-Ti latite and high-Ti and low Ti voluminous quartz latite eruptives. J. Petrol. 45, 107-138.
- Fuller R.R., 1931. The geomorphology and volcanic sequence of Steens Mountain in southeastern Oregon. Washington Univ Pub Geol 3, 1-130
- Frost, B.R., Barnes, C.G., Collins, W.J., Arculus, R.J., Ellis, D.J., Frost, C.R., 2001. A geochemical classification for granitic rocks. Jour. Petrol. 42, 2033-2048.

- Gunn B.M., Watkins N.D., 1970. Geochemistry of the Steens Mountain basalts, Oregon. *Geol. Soc. Am. Bull.*, 81, 1497-1516.
- Hart, W.K., Carlson, R.W., 1987. Tectonic controls on magma genesis and evolution in the northwestern United States. *J. Volcanol. Geoth. Res.*, 32 119-135.
- Hart, W.K., Aronson, J.L., Mertzman, S.A., 1984. Areal distribution and age of low-K, high-alumina olivine tholeiite magmatism in the northwestern Great Basin. *Geol. Soc. Am. Bull.* 95, 186-195.
- Hermann, U.R., Nelson, B.K., Ratschbacher, L.R., 1994. The origin of a terrane: the U/Pb systematics and tectonics of the Xolapa complex (southern Mexico). *Tectonics* 13, 455-474.
- Hildreth, W., 1979. The Bishop Tuff: Evidence for the origin of compositional zonation in silicic magma chambers. In: Chapin, C.E. & Elston, W.E. (eds), *Ash-flow tuffs*, *Geol. Soc. Am. Spec. Pap.*, 180, 43-75.
- Hildreth, W., 1981. Gradients in silicic magma chambers: Implications for lithospheric magmatism. *J. Geophys. Res.* 86, 10153-10192
- Hildreth, W., 2004. Volcanological perspective on Long Valley, Mammoth Mountain, and Mono Craters: several contiguous but discrete systems. *J. Volcanol. Geotherm. Res.* 136, 169-198.
- Hooper, P.R., Binger, G.B., Lees, K.R., Ages of the Steens and Columbia River flood basalts and their relationship to extension-related calcalkalic volcanism in eastern Oregon. *Geol. Soc. Am. Bull.* 114, 43-50.

- Honjo, N., Bonnicksen, B., Leeman, W.P., Stormer Jr, J.C., 1992. Mineralogy and geothermometry of high-temperature rhyolites from the central and western Snake River Plain. *Bull. Volcanol.* 54, 220-237.
- Humphreys E.D., Dueker K.G., Schutt D.L., Smith R.B., 2000. Beneath Yellowstone: Evaluating plume and nonplume models using teleseismic images of the upper mantle. *GSA. Today* 10, 1-7.
- Irvine, TN., Baragar, W.R.A., 1971. A guide to the chemical classification of the common volcanic rocks. *Can J. Earth Sci.* 8, 523-548.
- Johnson J.A., 1995, Geologic Evolution of the Cuck Creek Butte Eruptive Center, High Lava Plains, southeastern Oregon. Masters Thesis, Oregon State University, 151 pp.
- Johnson J.A., Grunder, A.L., 2000, The making of intermediate composition magma in a bimodal suite: Duck Butte Eruptive Center, Oregon, USA, *J Volc. Geoth. Res.* 95, 175-195.
- Johnson, J.A., Hawkesworth, C.J., Hooper, P.R., Binger, G.B., 1989. Major- and trace-element analyses of Steens Basalt, southeastern Oregon. *US Geol Surv Open-File Rep* 98-482, 1-25
- Johnson, D.M., Hawkesworth, C.J., Conrey, R.M., 1999. XRF analysis of rocks and minerals for major and trace elements on a single dilution Li-tetraborate fused bead. *Advances in X-ray analysis*, 41, 843-867.
- Johnson, M.C., Rutherford, M.J., 1989. Experimentally determined conditions in the Fish Canyon Tuff, Colorado, magma chamber. *J. Petrol.* 30, 711-737.
- Jordan, B.T., 2001, Tectonism and mafic volcanism of the High Lava Plains, eastern Oregon, Ph.D. Dissertation, Oregon State University.

- Jordan, B.T., Streck, M.J., Grunder, A.L., 2002. Bimodal volcanism and tectonism of the High Lava Plains, Oregon. In: Field Guide to Geologic Processes in Cascadia, Oregon. Dept. Geol. Min. Ind., Spec. Pap. 36, 23-46.
- Jordan, B. J., Grunder, A.L., Duncan R, Deino, A., 2004, Geochronology of age-progressive volcanism of the Oregon High Lava Plains: Implications for the plume interpretation of Yellowstone. *J Geophys. Res.* 109, B10202, doi10.10292003JB002776.
- Kirsten, L.A., Peate, D.W., Hawkesworth, C.J., Turner, S.P., Harris, C., Mantovani, S.M., 2000. Early Cretaceous basaltic and rhyolitic magmatism in southern Uruguay associated with the opening of the south Atlantic. *Jour. Petrol.* 41, 1413-1438.
- Lindsay, J.M., Schmitt, A.K., Trumbull, R.B., DeSilva, S.L., Siebel, W., Emmermann, R., 2001. Magmatic evolution of the La Pacana caldera system, central Andes, Chile: Compositional variation of two cogenetic large-volume felsic ignimbrites. *J. Petrol.*, 42, 459-486.
- Linneman, S.K., Myers, J.D. 1990. Magmatic inclusions in the Holocene rhyolites of Newberry volcano, central Oregon. *J. Geoph. Res.* 95, 17,677-17.691.
- Lipman, P.W., 2000. Central San Juan caldera cluster: Regional volcanic framework. *Geol. Soc. Am. Special Paper* 346, 9-69.
- Lu, F., 1991. The Bishop Tuff: origins of the high-silica rhyolite and its thermal and chemical zonation. Ph.D. dissertation, University of Chicago, 313 pp.
- MacLean J.W., 1994, Geology and geochemistry of Juniper Ridge, Horsehead Mountain and Burns Butte: Implications for the petrogenesis of silicic magma on the High Lava Plains, southeastern Oregon. Master's thesis, Oregon State Univ, Corvallis, Oregon, pp 141.

- MacLeod N.S., Walker G.W., McKee E.H., 1976. Geothermal significance of eastward increase in age of upper Cenozoic rhyolitic domes in southeastern Oregon. Second United Symposium on the development and use of geothermal resources, Proceedings 1: 465-474.
- Mahood, G.A., 1981. Chemical evolution of a Pleistocene rhyolitic center: Sierra La Primavera, Jalisco, Mexico. *Contrib. Mineral. Petrol.*, 77, 129-149.
- Matthews, A., Palin, J.M., Epstein, S., Stolper, E.M. 1994. Experimental study of $^{18}\text{O}/^{16}\text{O}$ partitioning between crystalline albite, albitic glass, and CO_2 gas. *Geochim. Cosmochim. Acta* 58, 5255-5266.
- Maughan, L.L., Christiansen, E.H., Best, M.G., Gromme, C.S., Deino, A.L., Tingey, D.G., 2002. The Oligocene Lund Tuff, Great Basin, USA: a very large volume monotonous intermediate. *J. Volc. Geotherm. Res.* 113, 129-157.
- Michael, P.J., 1983, Chemical differentiation of the Bishop Tuff and other high-silica magmas through crystallization processes. *Geology* 11, 31-34.
- Mills, J.G, Saltoun, B.W., Vogel, T.A., 1997. Magma batches in the Timber Mountain magmatic system, southwestern Nevada volcanic field, Nevada, USA. *J. Volcan. Geoth. Res.* 78, 185-208.
- Miller C.F., Watson, E.B., Harrison, T.M., 1988. Perspectives on the source, segregation and transport of granitoid magmas. *Trans. Roy. Soc. Edinburgh, Earth Sciences*, 79, 135-156.
- Nelson, B.K., 1995. Fluid flow in subduction zones: evidence from Nd- and Sr-isotope variations in metabasalts of the Franciscan Complex, California. *Contrib. Mineral. Petrol.*, 119, 247-262.
- Pearce, J.A, 1984. Trace element discrimination diagrams for the tectonic interpretation of granitic rocks. *J. Pet.* 25, 956-983.

- Pendergast, K. J., Grunder, A. L., and Haggerty, R., 2000, Diffusion in banded pumice: Constraints on eruption rates of ignimbrites and elemental diffusivities, *Geol. Soc. Am., Abst. Prog.*, 32, pp.500.
- Perkins, M.E., Nash, B.P., 2002. Explosive silicic volcanism of the Yellowstone hotspot: the ash fall tuff record. *Geol. Soc. Am. Bull.* 114, 367-381.
- Pierce, K.L., Morgan, L.A., 1992, The track of the Yellowstone hotspot: volcanism, faulting, and uplift. In: Link, P.K., Kuntz, M.A., Platt, L.B., eds., *Regional Geology of eastern Idaho and western Wyoming*. *Geol. Soc. Am. Memoir* 179, 1-53.
- Sawka, W.N., Chappell, B.W., Kistler, R.W., 1990. Granitoid compositional zoning by side-wall boundary layer differentiation: evidence from the Palisade Crest intrusive suite, central Sierra Nevada, California. *J. Petrol.* 31, 519-553.
- Scaillet, B., MacDonald, R., 2001. Phase relations of peralkaline silicic magmas and petrogenetic implications. *J. Petrol.* 42, 825-845.
- Sisson, T.W., Ratajeski, K., Hankins, W.B., Glazner, A.F., 2005. Voluminous granitic magmas from common basaltic sources. *Contrib. Mineral Petrol.* 148, 635-661.
- Skjerlie, K.P., Johnston, A.D., 1992. Vapor-absent melting at 10 kbar of a biotite- and amphibole-bearing tonalitic gneiss: implications for the generation of A-type granites, *Geology*. 20, 263-266.
- Skjerlie, K.P., Johnston, A.D., 1993. Fluid-absent melting behavior of an F-rich tonalitic gneiss at mid-crustal pressures: Implications for the generation of anorogenic granites, *Jour. Petrol.* 34, 785-815.
- Sparks, R.S.J., Huppert, H.E., and Turner, J.S., 1984. The fluid dynamics of evolving magma chambers. *Philos. Trans. Roy Soc. London*, A310, 511-534.

- Streck, M.J., 2002. Partial melting to produce high-silica rhyolites of a young bimodal suite: compositional constraints among rhyolites, basalts, and metamorphic xenoliths from the Harney Basin, Oregon. *Int. J. Earth. Sci.* 91, 583-593.
- Streck, M.J., Grunder A.L., 1995. Crystallization and welding variations in a widespread ignimbrite sheet: The Rattlesnake Tuff, eastern Oregon. *Bull. Volcanol.* 57, 151-169
- Streck, M.J., Grunder, A.L. 1997. Compositional gradients and gaps in high-silica rhyolites of the Rattlesnake Tuff, Oregon. *J. Petrol.* 38, 133-163
- Streck M.J., Grunder A.L., 1999. Enrichment of basalt and mixing of dacite in the rootzone of a large rhyolite chamber: inclusions and pumices from the Rattlesnake Tuff, Oregon. *Contrib. Mineral. Petrol.* 136, 193-212
- Streck, M.J., Grunder, A.L., 2002. Processes relating trachy- and calc-alkaline intermediate rocks to primitive tholeiite within a strongly divergent suite from Harney Basin, Oregon. *Geol. Soc. Am. Sbsst. Prog.* 34, pp. 38.
- Taylor, H.P., Jr., 1968. The oxygen isotope geochemistry of igneous rocks. *Contrib. Mineral. Petrol.*, 19, 1-71.
- Taylor, H.P., Jr., Sheppard, S.M.F., 1986. Igneous rocks: I. Processes of isotopic fractionation and isotope systematics. In: Valley, J.W., Taylor, H.P. Jr., O'Neil, J.R., eds, *Stable isotopes in high temperature geological processes.* *Rev. Mineral.* 16, 227-273.
- Walker G.W., 1979. Revisions to the Cenozoic stratigraphy of Harney Basin, southeastern Oregon. *US Geol Surv Bull* 1475, 1-35.
- Walker, GW , 1981. Uranium, thorium and other metal associations in silicic volcanic complexes of the northern Basin and Range, a preliminary report. *US Geol. Surv. Open-File Report*, 81-1290, 45pp.

Whalen J.B., Currie, K.L., Chappell, B.W., 1987. A-type granites: geochemical characteristics, discrimination, and petrogenesis. *Contrib. Mineral. Petrol.* 95, 407-419.

Whitney, J.A., Stormer, J.C., 1985. Mineralogy, petrology, and magmatic conditions from the Fish Canyon Tuff, central San Juan volcanic field, Colorado. *J.Pet.*, 26, 726-262.

Wilson C.J.N., Houghton, B.F., Kamp, P.J.J., McWilliams, M.O., 1995. An exceptionally widespread ignimbrite with implications for pyroclastic flow emplacement. *Nature* 378, 605-607.

Figure and Table captions:

Table 1. RST = Rattlesnake Tuff, JR = Juniper Ridge. 1. sample 210.1b is a single small inclusion and data are exclusively INAA data except P by electron microprobe and Si by difference to 100% ; 2. Formerly known as Squaw Butte. Ages from Jordan et al. (2004), except RST (Streck and Grunder, 1995) and 209an (Streck, unpublished). All RST samples assigned RST age. 93.1 cuts RST and is overlain by 6.85-Ma tuff of Buckaroo Lake. JR-92-53 overlies Juniper Ridge, west. XRF analyses done at Geoanalytical Laboratories, Washington State University, Pullman WA (See Johnson et al, 1999). Samples 210.1b has only neutron activation analyses trace elements. Instrumental neutron activation analysis was done at Oregon State University using 1 MW Triga reactor and counting facilities (see Streck and Grunder, 1997 for details); 'n.d.' = not detected; empty space = not analyzed. Isotope dilution and isotope analyses were conducted at the University of Washington. Sample preparation and analytical procedure performed in accordance with Herrmann et al. (1994) and Nelson (1995). Duplicate $^{143}\text{Nd}/^{144}\text{Nd}$ and ϵ_{Nd} values for sample JR-91-21 are 0.512882 and 4.8, respectively. Duplicate $^{206}\text{Pb}/^{204}\text{Pb}$, $^{207}\text{Pb}/^{204}\text{Pb}$, and $^{208}\text{Pb}/^{204}\text{Pb}$ values

for sample JR-92-53 are 18.784, 15.572, and 38.389; for sample HP-91-2 they are 18.877, 15.637, and 38.586; for sample JR-92-62 they are 18.863, 15.608, and 38.595.

Table 2: Bulk composition of hand-picked mineral separates. Details about separates and analytical techniques are found in Streck and Grunder (1997).

Fig. 1: a) Regional setting and outcrop pattern of the Rattlesnake Tuff in Oregon. Gray shows outline of High Lava Plains and black shows generalized Rattlesnake Tuff outcrops; proposed source shown by cross. Inferred pre-eruptive outcrop area shown by solid envelope around outcrops (Streck and Grunder, 1995) Solid lines with numbers are simplified isochrons in million of years for NW-migrating silicic volcanism, after MacLeod et al. (1976) as refined by Jordan et al. (2002). Fine solid lines indicate faults (shown only for area east of the Cascades) and stars indicate Cascade composite volcanoes. b) Analyses of 286 volcanic rocks from the High Lava Plains define a bimodal distribution of compositions, of mostly basaltic and rhyolitic rocks. Intermediate rocks (only 7% andesites and dacites) were likely disproportionately “oversampled” because of petrologic significance, after Jordan et al. (2002). Data source: MacLean (1994), Streck and Grunder (1997, 1999), Johnson and Grunder (2000), Jordan et al. (2002) and unpublished data of Grunder and Streck.

Fig. 2: Trace elemental composition of Rattlesnake Tuff samples. Main panels show variations within high-silica rhyolites and insets show compositional relationships among high-silica rhyolites, dacites, and basaltic andesitic to basaltic inclusions (data from Streck and Grunder, 1997, 1999). Distinct rhyolite compositions, labeled A through E in panel (a), are

defined by clustering of pumices analyses based on 4 to 7 analyses per group. In panel (b), silica composition of rhyolite group averages (± 1 standard deviation) and silica ranges for dacites and cognate basaltic andesitic basaltic inclusions are superimposed. Numbers in panel (e) are Ba and Eu concentrations in alkali-feldspar separates, respectively. Symbols for all panels are as indicated in panel (a).

Fig. 3: Bulk compositions of mineral separates in comparison with single point microprobe analyses of Rattlesnake Tuff rhyolites B through E (see also Table 2); A is aphyric. Bulk mineral composition, i.e. averaged mineral composition over a large number of crystals, is distinct for each RST rhyolites while single point analyses are more transitional between adjacent rhyolite compositions. We randomly associated a single alkali-feldspar analysis with one clinopyroxene and one titanomagnetite analysis for the shown plot.

Fig. 4 : Nd, Sr, and Pb isotopic variations among Rattlesnake Tuff compositions (RST rhyolites, RST mafic inclusions (inc) and RST dacites), other High Lava Plain rhyolites (Burns Butte and Juniper Ridge (JR)), high-alumina basalts (HAOT; 93.1ba, JR92-53) and basaltic andesitic composition with calcalkaline character (calc.; 209an) and trachyandesite (trachy; JR-91-21) with tholeiitic character (see Table 1).

Fig. 5: Microprobe traverse data for clinopyroxene and alkali-feldspar phenocrysts of rhyolite groups B through E (rhyolite A is aphyric). Analysis traverses go from center (left) to rim (right) of grains; vertical bar marks the rim of each grain (data from this study). Rim to center traverses range in length from 220 to 616 microns and the step length is 12 to 32 microns.

Fig. 6.: Scatter diagram of alkali-feldspar (top) and clinopyroxene (bottom) mineral compositions (data from this study, as shown in Fig. 5). Compositional overlap of a subset of data points of group E alkali-feldspars and clinopyroxene with group D and overlap between clinopyroxene of D and C suggest either inheritance or similar growth conditions existed

Fig. 7: Compositional variation of Harney Basin rhyolites (data sources: MacLean, 1994, Streck and Grunder 1997, this study) and select other calcalkaline varieties; BT = Bishop Tuff (Hildreth, 1981), VTTS = Tuff of Valley of Ten Thousand Smokes (Hildreth, 1981), San Luis rhyolites = representative analyses (Streck et al., unpubl. data) of rhyolitic lavas and tuffs from the San Luis caldera complex, San Juan volcanic field (Lipman, 2000). All analyses belonging to Rattlesnake Tuff rhyolite E were plotted to illustrate the homogeneity among least-evolved rhyolite samples but only group averages are plotted for the more evolved rhyolites D through A for clarity.

Fig. 8: FeO* versus TiO₂ (wt.%) of interstitial glasses of monotonous intermediate tuffs compared to glass and aphyric bulk compositions of high-silica rhyolites of the Rattlesnake Tuff E and other selected rhyolites from bimodal provinces. All data normalized to 100% volatile free. Non-Rattlesnake Tuff (RST) data sources are (in order of legend): Perkins and Nash, 2002; Cathey and Nash, 2004, Mahood, 1981; Bachmann et al., 2002; Johnson and Rutherford, 1989, E, Christiansen, pers. communication; Lindsay et al., 2001; and Lu, 1991.

Fig. 9: Sr vs. Ba diagram with observed Rattlesnake rhyolite (average) compositions and calculated models. X = fraction of plagioclase in a fractionating feldspar assemblage. We assumed observed variation between composition E and A is solely due to sanidine fractionation and thus calculations model the addition of plagioclase to an initial pure sanidine fractionation scenario ($X=0$). Partition coefficients for Sr and Ba in plagioclase were calculated for An_{30} plagioclase using the Blundy and Wood (1991) formulation. D_{Ba} and D_{Sr} in sanidine are based on required fractionation amounts as inferred by enrichment of elements taken as perfectly incompatible and elemental variations of Ba and Sr between rhyolite E and A (cf., Streck and Grunder, 1997). D_{Ba} is 7.5 and D_{Sr} is 4.7. Tic marks are at 5% fractionation increments. Rhyolite at highest Ba and Sr is rhyolite E, and A at lowest Ba, Sr.

Table 1. Analyses of samples from western Harney Basin, High Lava Plains, OR.

| sample no. sample info | MAFIC | | ROCKS | | | SILICIC | | ROCKS | | | |
|--|---|----------------|---------------|---|------------------------|------------------------------------|-----------------------------|-----------------------------|--------------------------|---------------------------------|---------------------------------|
| | 210.1b ¹ RST inclusion | 93.1ba lava | 209an lava | JR-91-21 Paiute Butte ² lava | JR-92-53 JR lava | HP-91-2 Burns Butte obsidian | RT-173h RST, A pumice | RT-173c RST, E pumice | RT-211a RST pumice | JR-92-48 JR east obsidian | JR-92-62 JR west obsidian |
| latitude, °N | | 43.131 | | 43.475 | 43.485 | 43.553 | 43.151 | | | 43.510 | 43.517 |
| longitude, °W | | 119.9416 | | 119.720 | 119.538 | 119.250 | 119.7028 | 119.7028 | | 119.577 | 119.755 |
| age info (Ma) | 7.1 | ≤7.1 | 6.7 | 2.4 | <5.7 | 7.7 | 7.1 | 7.1 | 7.1 | 6.9 | 5.7 |
| XRF analyses, normalized 100% volatile free weight % | | | | | | | | | | | |
| SiO ₂ | 53.9 | 48.47 | 57.76 | 54.64 | 48.19 | 74.34 | 77.74 | 75.64 | 65.57 | 72.74 | 75.24 |
| TiO ₂ | 2.4 | 0.99 | 1.23 | 1.74 | 1.58 | 0.22 | 0.11 | 0.16 | 1.16 | 0.28 | 0.17 |
| Al ₂ O ₃ | 13.8 | 16.69 | 16.25 | 14.87 | 16.57 | 13.33 | 11.97 | 12.29 | 13.16 | 14.30 | 13.37 |
| FeO* | 11.4 | 10.22 | 7.44 | 12.76 | 10.76 | 1.59 | 0.78 | 1.96 | 6.30 | 1.98 | 1.57 |
| MnO | 0.40 | 0.20 | 0.14 | 0.39 | 0.19 | 0.05 | 0.08 | 0.10 | 0.21 | 0.05 | 0.05 |
| MgO | 4.2 | 8.88 | 4.25 | 2.16 | 9.24 | 0.19 | 0.05 | 0.01 | 1.98 | 0.63 | 0.15 |
| CaO | 6.3 | 11.75 | 6.50 | 5.64 | 9.91 | 0.61 | 0.26 | 0.51 | 3.73 | 2.19 | 1.03 |
| Na ₂ O | 3.62 | 2.45 | 3.94 | 4.69 | 2.91 | 4.59 | 3.46 | 4.62 | 4.06 | 3.62 | 4.49 |
| K ₂ O | 2.7 | 0.23 | 2.15 | 2.10 | 0.32 | 5.04 | 5.53 | 4.70 | 3.21 | 4.14 | 3.91 |
| P ₂ O ₅ | 1.3 | 0.11 | 0.35 | 1.01 | 0.32 | 0.04 | 0.02 | 0.01 | 0.61 | 0.07 | 0.02 |
| Total | | 100.33 | 100.13 | 98.21 | 99.99 | 99.18 | 99.90 | 99.5 | 99.96 | 99.57 | 99.19 |
| ppm | | | | | | | | | | | |
| Rb | 45 | 1.6 | 42 | 34 | 2.7 | 115 | 122 | 64 | 55 | 107.4 | 90.1 |
| Ba | 1182 | 156 | 813 | 1552 | 270 | 670 | 39 | 1835 | 1210 | 1189 | 1558 |
| Sr | | 383 | 272 | 255 | 277 | 27 | 2 | 23 | 146 | 157 | 74 |
| Zr | | 51 | 255 | 834 | 107 | 293 | 175 | 457 | 419 | 196 | 251 |
| Nb | | 1 | 12 | 55 | 5 | 32 | 39 | 26 | 24 | 10 | 11 |
| Y | | 24 | 38 | 130 | 28 | 41 | 100 | 76 | 76 | 23 | 44 |
| Pb | | 2 | 9 | 12 | 2 | 17 | 20 | 10 | 45 | 14 | 16 |
| Zn | | 73 | 79 | 211 | 97 | 40 | 88 | 113 | 162 | 32 | 45 |
| Ga | | 17 | 19 | 27 | 18 | 16 | 18 | 19 | 19 | 13 | 15 |
| V | | 262 | 154 | 7 | 243 | 3 | nd | 2 | 76 | 16 | 3 |
| Cu | | 120 | 42 | 15 | 71 | 7 | 1 | 5 | 18 | 8 | 4 |
| Ni | | 143 | 47 | 14 | 175 | 5 | 14 | 9 | 17 | 7 | 8 |
| Cr | | 237 | 67 | n.d. | | 0.9 | n.d. | 0.3 | 16 | n.d. | n.d. |
| INA analyses | | | | | | | | | | | |
| Cs | 1.6 | 0.4 | 1.9 | 0.4 | n.d. | 3.3 | 4.5 | 2.4 | 2.6 | 4.8 | 2.6 |
| U | n.d. | n.d. | 1.7 | 1.8 | n.d. | 5.2 | 4.9 | 2.2 | 1.8 | 4.5 | 3.4 |
| Th | 2.5 | 0.2 | 4.3 | 3.3 | 0.4 | 10.1 | 9.5 | 5.7 | 4.5 | 10.1 | 8.2 |
| Hf | 7.2 | 1.4 | 5.9 | 17.2 | 2.8 | 8.0 | 7.1 | 11.1 | 9.5 | 5.7 | 7.0 |
| Ta | 1.06 | 0.08 | 0.73 | 2.77 | 0.23 | 1.90 | 2.16 | 1.35 | 1.32 | 0.84 | 0.74 |
| Sc | 41.3 | 47.5 | 21.7 | 43 | 32 | 3.8 | 3.9 | 4.3 | 22.6 | 5 | 4.8 |
| Co | 19.2 | 49.7 | 24.5 | 8.1 | 52 | 1.1 | 0.1 | 0.1 | 9.8 | 3.3 | 0.7 |
| Cr | 27 | 280 | 76 | 3 | 279 | 1.6 | n.d. | 1.8 | 23 | 5 | |
| La | 34.2 | 3.4 | 19.2 | 59 | 8.0 | 40.8 | 19.9 | 52 | 35.7 | 22.4 | 27.2 |
| Ce | 77 | 8.0 | 40 | 141 | 19 | 81 | 49 | 112 | 86 | 44 | 63 |
| Nd | 48 | 8.6 | 21 | 74 | 15 | 34 | 28 | 58 | 48 | 18.7 | 28.2 |
| Sm | 14.1 | 2.42 | 5.6 | 19.5 | 4.0 | 6.3 | 9.6 | 13.4 | 12.1 | 3.5 | 5.6 |
| Eu | 5.24 | 0.98 | 1.68 | 6.1 | 1.56 | 0.44 | 0.65 | 2.48 | 3.45 | 0.69 | 1.16 |
| Tb | 2.3 | 0.62 | 0.98 | 3.5 | 0.81 | 1.0 | 2.2 | 2.1 | 2.1 | 0.55 | 0.95 |
| Yb | 7.2 | 2.8 | 3.8 | 13.6 | 2.6 | 4.5 | 10.5 | 7.9 | 7.4 | 2.7 | 4.8 |
| Lu | 1.08 | 0.40 | 0.54 | 1.89 | 0.38 | 0.70 | 1.61 | 1.23 | 1.10 | 0.44 | 0.69 |
| Isotope dilution | | | | | | | | | | | |
| Rb | 31.79 | | 41.8 | | | 78.708 | 123.51 | 61.269 | 53.308 | 102.87 | 88.704 |
| Sr | 264.4 | | 265.0 | | | 22.979 | 1.8029 | 22.561 | 144.64 | 153.55 | 72.313 |
| ⁸⁷ Rb/ ⁸⁶ Sr | 0.3480 | 0.0205 | 0.4569 | 0.3864 | 0.0282 | 9.9126 | 198.26 | 7.8592 | 1.0666 | 1.9388 | 3.5500 |
| ¹⁴³ Nd/ ¹⁴⁴ Nd | 0.51282 | 0.51292 | 0.51285 | 0.51290 | 0.51292 | 0.51276 | 0.51284 | 0.51282 | 0.51282 | 0.51282 | 0.51287 |
| εNd _t | 3.5 | 5.4 | 4.0 | 5.1 | 5.4 | 2.4 | 4.0 | 3.5 | 3.6 | 3.5 | 4.5 |
| ⁸⁷ Sr/ ⁸⁶ Sr | 0.70414 | 0.70364 | 0.70390 | 0.70365 | 0.70366 | 0.70718 | 0.72498 | 0.70510 | 0.70415 | 0.70394 | 0.70409 |
| ⁸⁷ Sr/ ⁸⁶ Sr _i | 0.70410 | 0.70363 | 0.70386 | 0.70362 | 0.70358 | 0.70608 | 0.70499 | 0.70431 | 0.70404 | 0.70375 | 0.70380 |
| ²⁰⁶ Pb/ ²⁰⁴ Pb | 18.798 | 18.844 | 18.824 | 18.816 | 18.805 | 18.874 | 18.849 | 18.847 | 18.814 | 18.816 | 18.865 |
| ²⁰⁷ Pb/ ²⁰⁴ Pb | 15.585 | 15.601 | 15.599 | 15.589 | 15.590 | 15.618 | 15.620 | 15.622 | 15.604 | 15.569 | 15.614 |
| ²⁰⁸ Pb/ ²⁰⁴ Pb | 38.417 | 38.462 | 38.502 | 38.481 | 38.438 | 38.624 | 38.535 | 38.547 | 38.480 | 38.399 | 38.504 |

| | <u>Feldspar</u> * | | <u>Pyroxene</u> * | | | <u>Ti-Magnetite</u> * | |
|-----------|---------------------------|-----------|-------------------|-------------|-----------|--------------------------|-----------|
| Rhyolite: | Na ₂ O wt.% | Ba ppm | FeO* wt.% | MnO wt.% | Sc ppm | TiO ₂ wt.% | Ta ppm |
| E | 8.8 | 12300 | 28.8 | 2.2 | 361 | 19.4 | 4.9 |
| D | 8.1 | 11000 | 26.4 | 2.5 | 385 | 17.0 | 4.7 |
| C | 6.4 | 5700 | 24.5 | 2.7 | 467 | 14.1 | 3.1 |
| B | 5.8 | 2600 | 21.3 | 3.0 | 496 | 11.0 | 2.5 |

* Each mineral composition is a composite of 50-300 crystals

Table 2: bimodal rhyolites & RST, Streck and Grunder

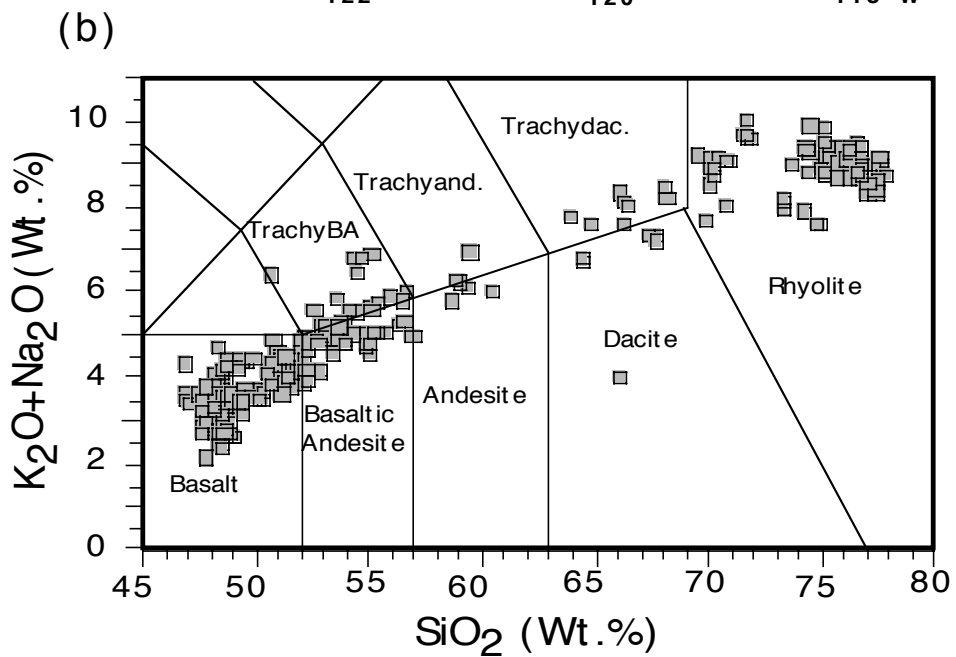
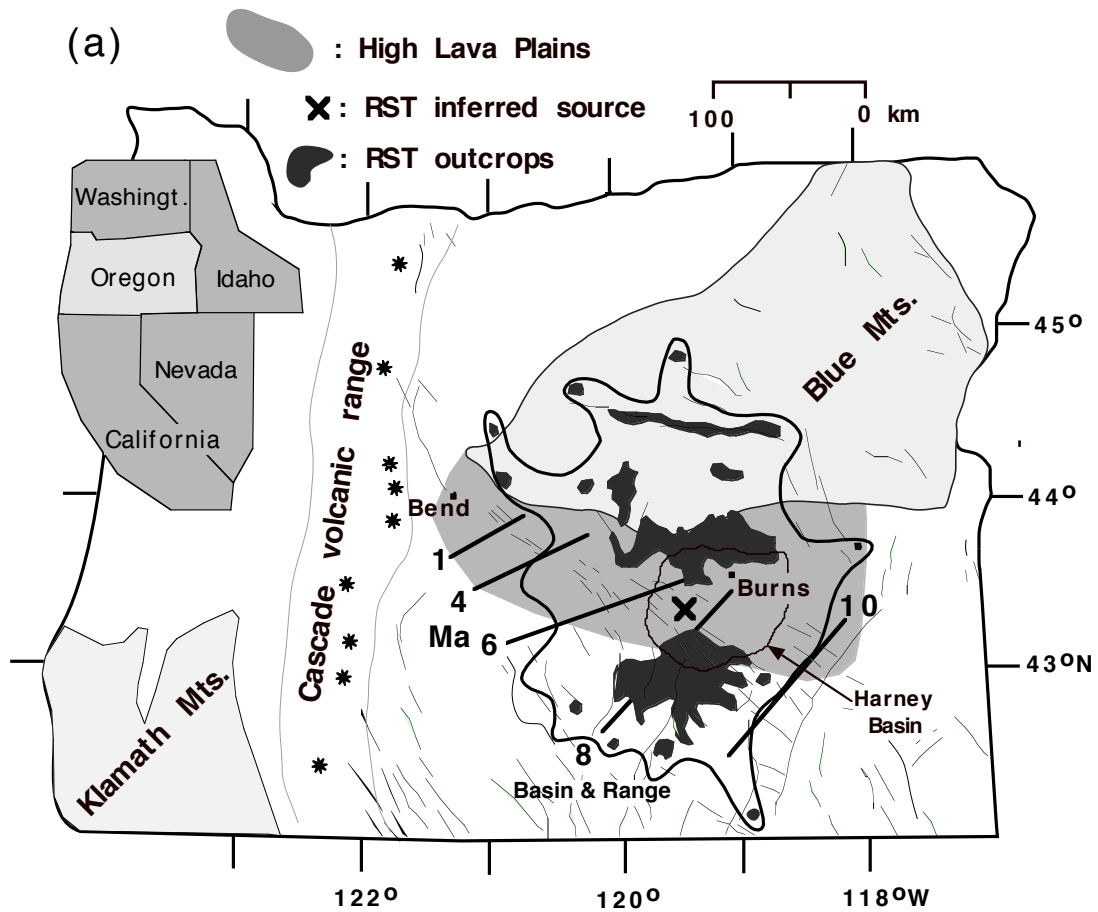


Fig. 1, bimodal rhyolites & RST, Streck and Grunder

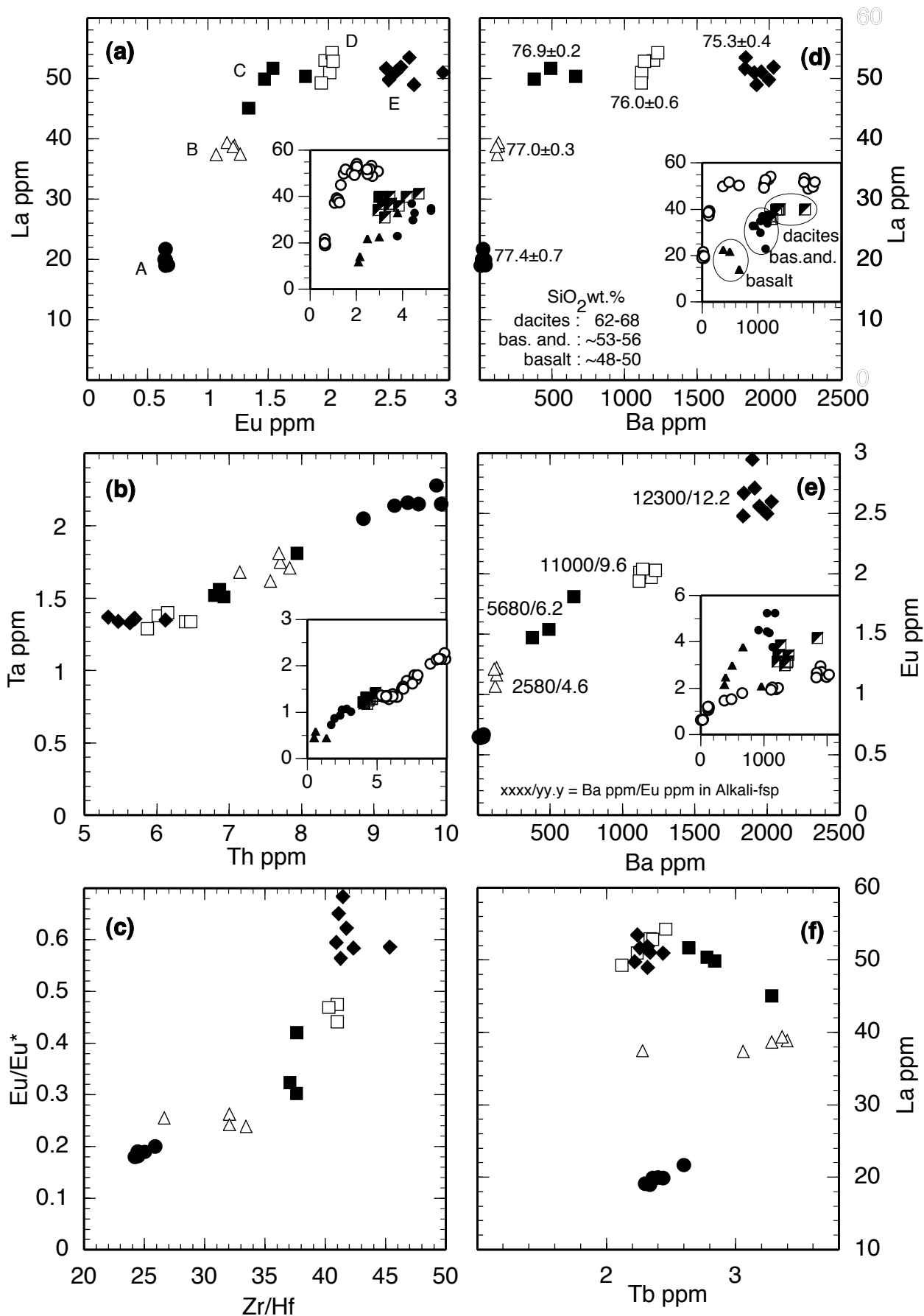


Fig. 2 : bimodal rhyolites & RST, Streck and Grunder

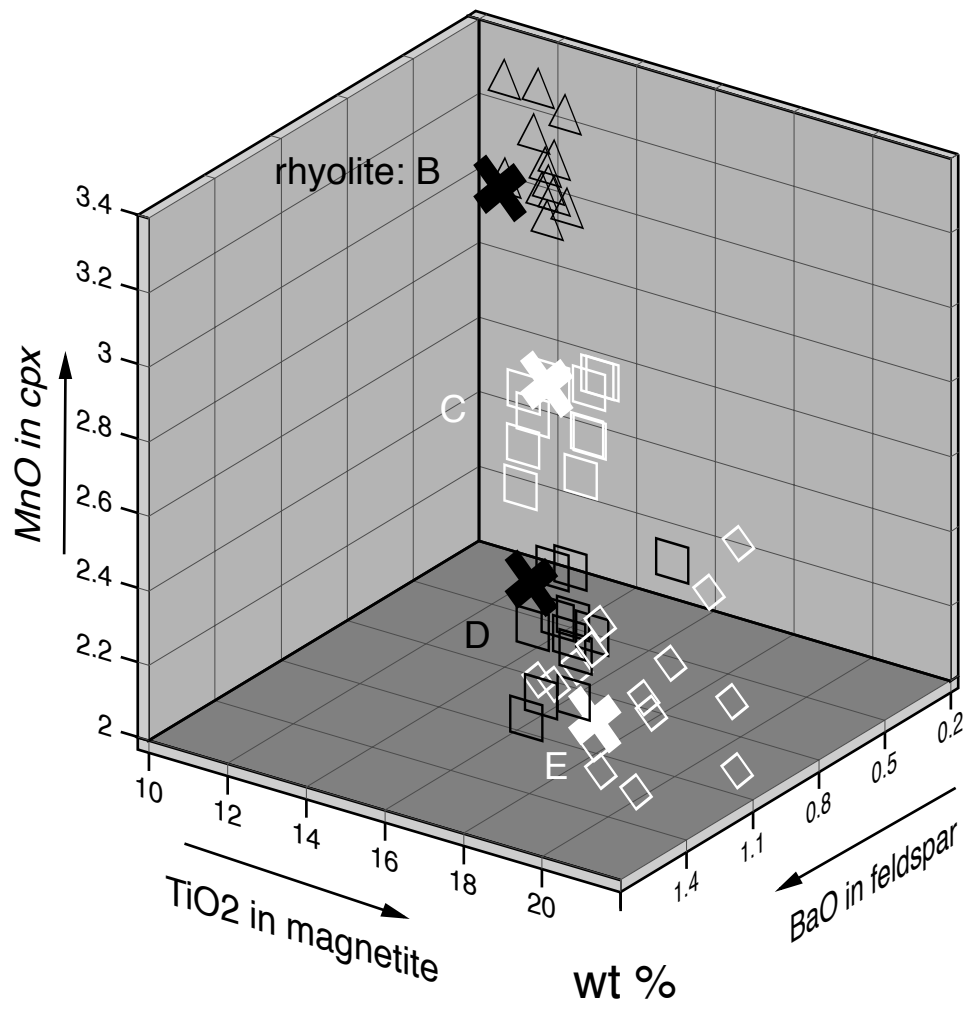


Fig. 3: bimodal rhyolites & RST, Streck and Grunder

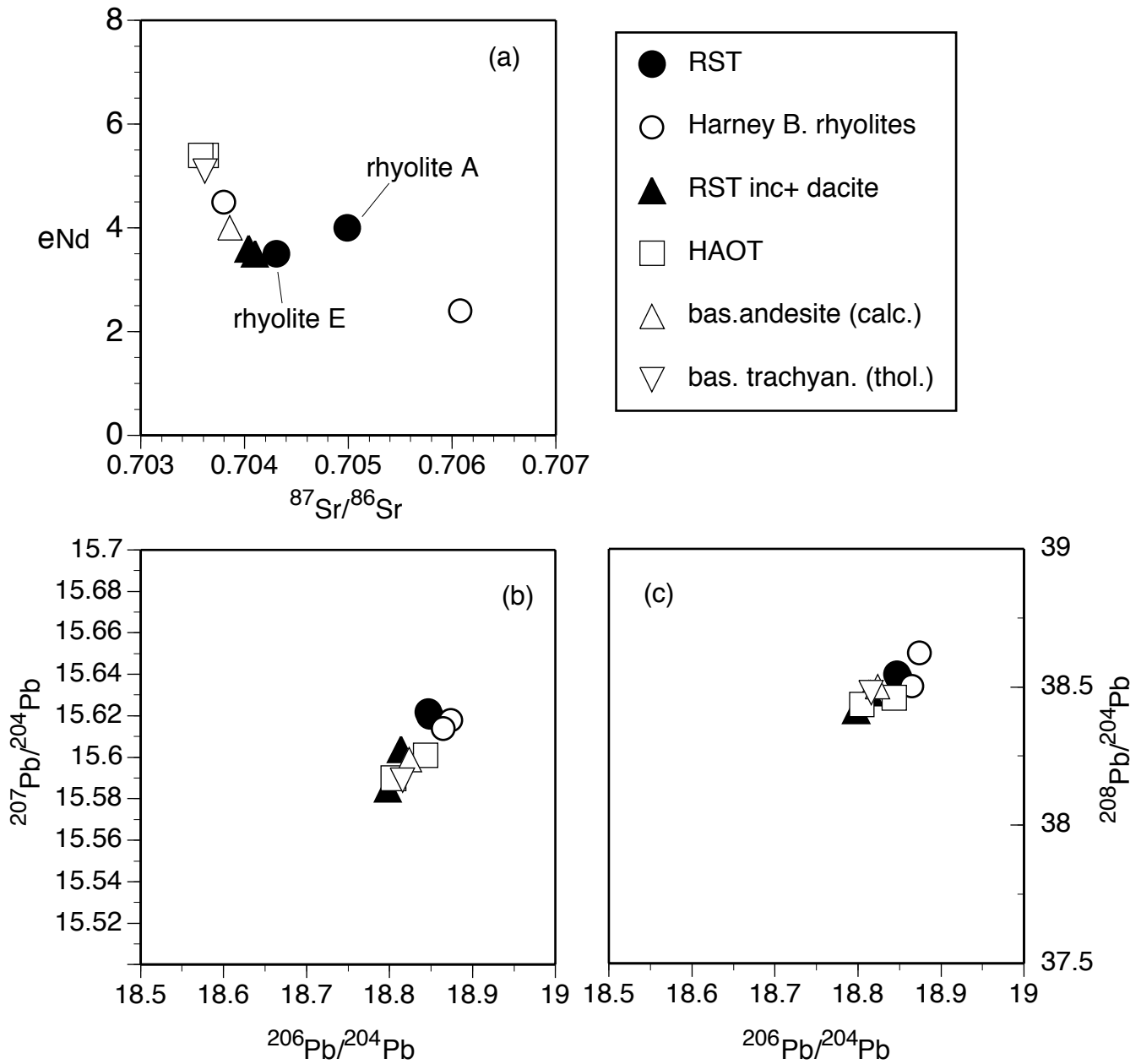


Fig. 4, bimodal rhyolites & RST, STreck and Grunder

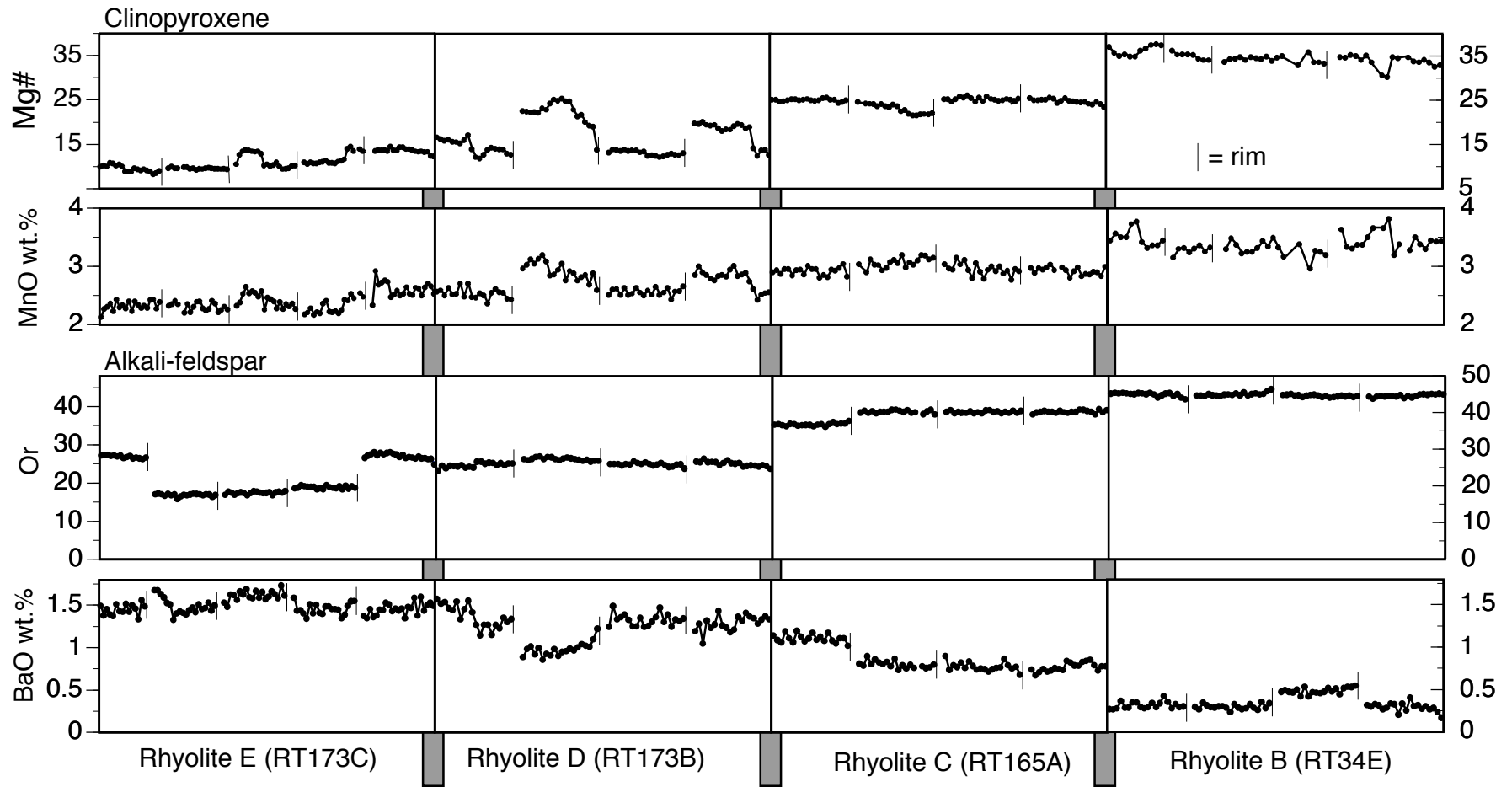


Fig. 5, bimodal rhyolites & RST, Streck and Grunder

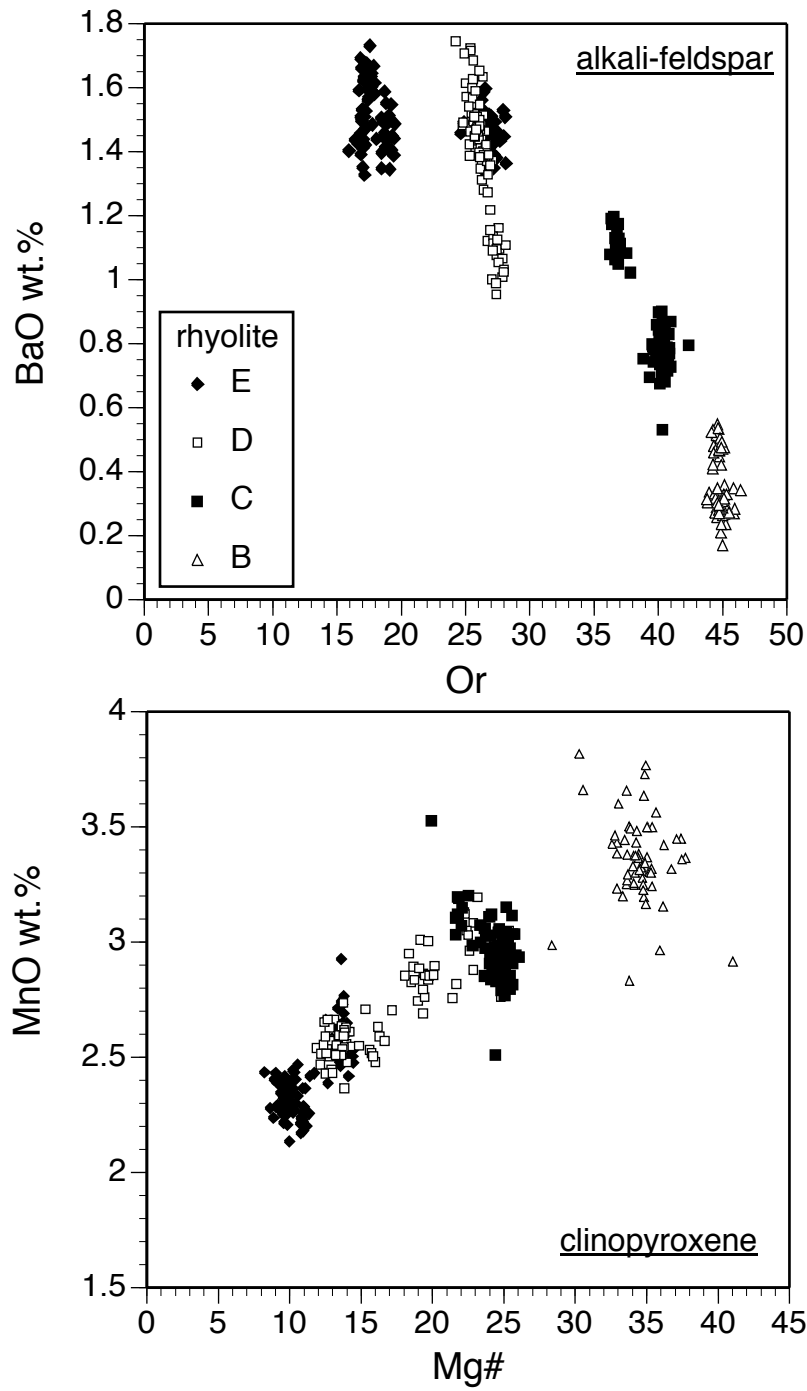


Fig. 6, bimodal rhyolites & RST, Streck and Grunder

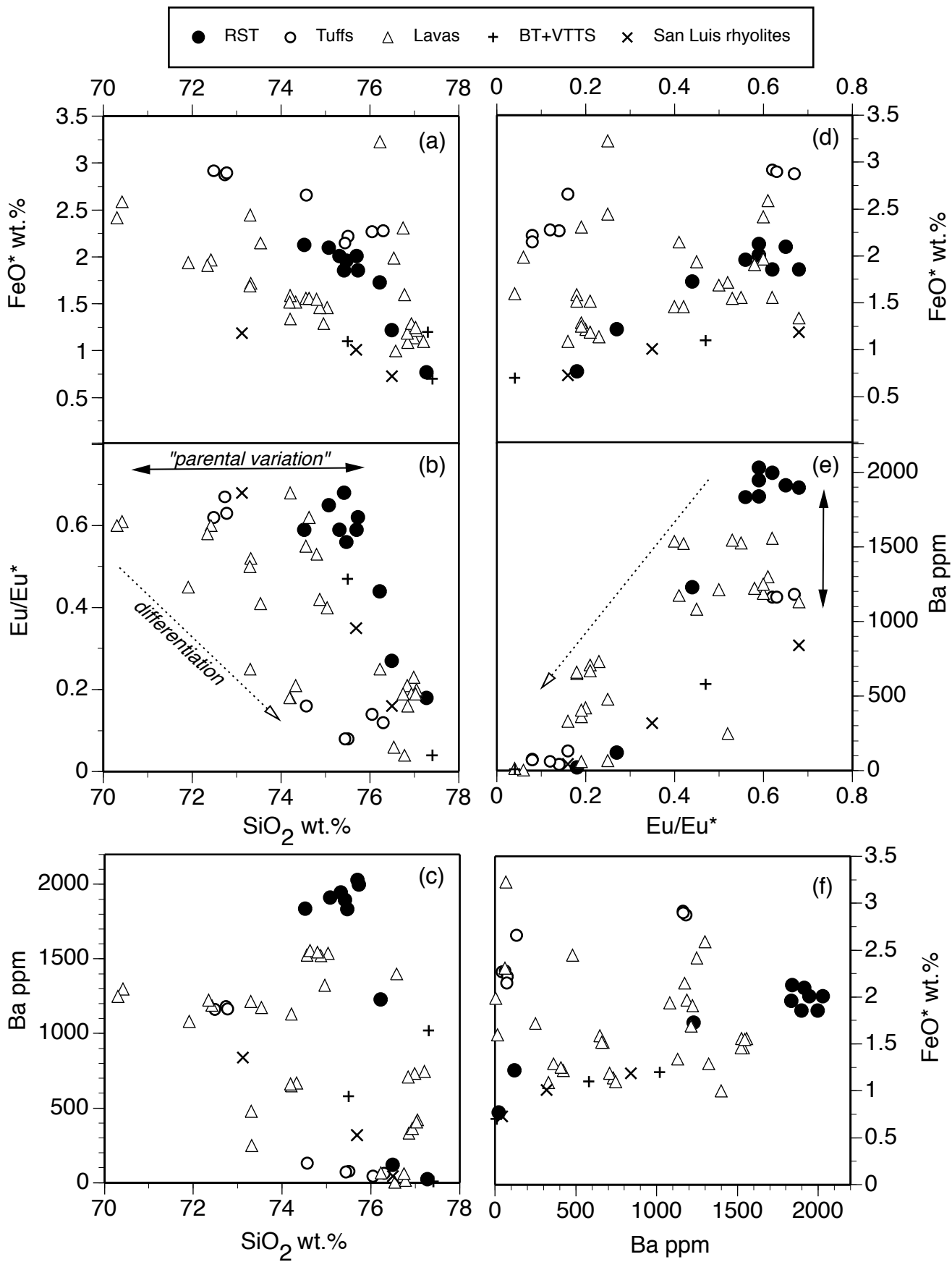


Fig. 7, bimodal rhyolites & RST, Streck and Grunder

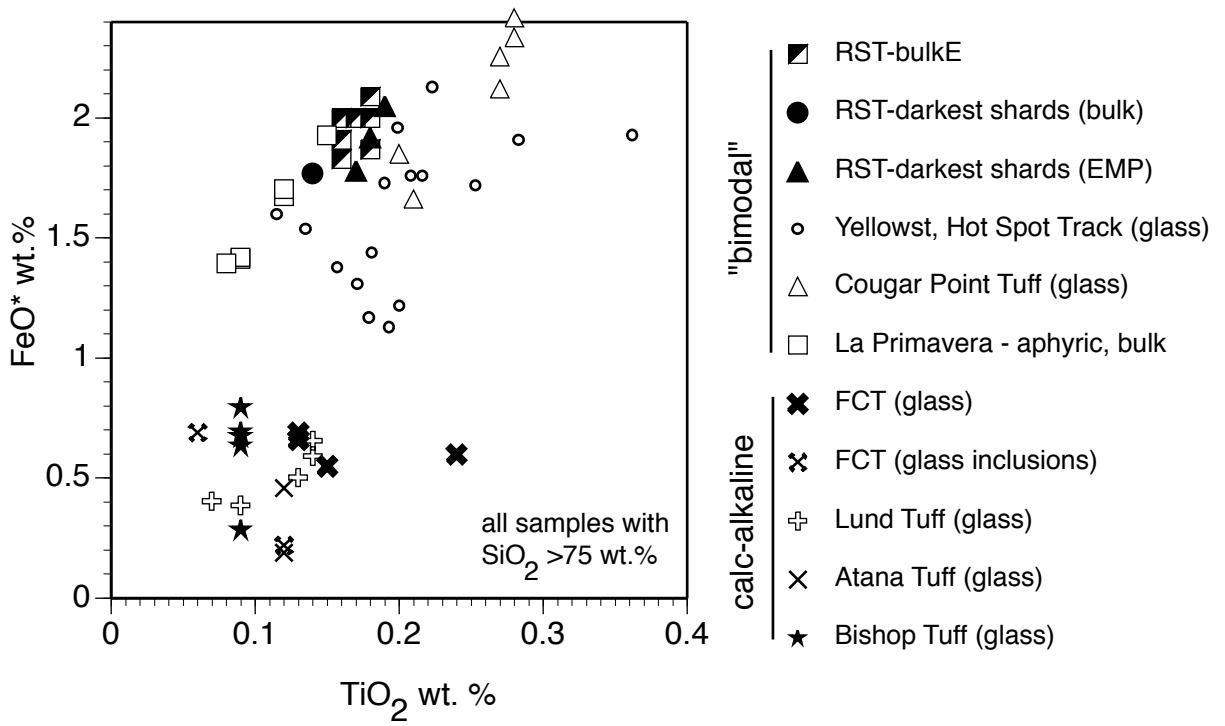


Fig. 8, bimodal rhyolites & RST, Streck and Grunder

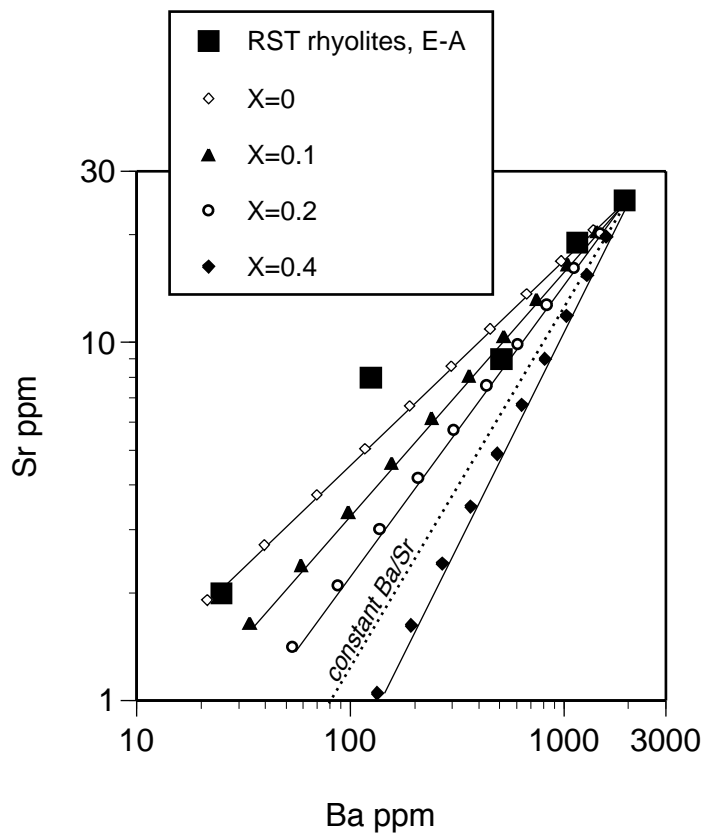


Fig. 9, bimodal rhyolites & RST, Streck and Grunder